Power Management and Power Flow Control With Back-to-Back Converters in a Utility Connected Microgrid

Ritwik Majumder, *Student Member, IEEE*, Arindam Ghosh, *Fellow, IEEE*, Gerard Ledwich, *Senior Member, IEEE*, and Firuz Zare, *Senior Member, IEEE*

***Abstract*—This paper proposes a method for power flow control between utility and microgrid through back-to-back converters, which facilitates desired real and reactive power flow between utility and microgrid. In the proposed control strategy, the system can run in two different modes depending on the power requirement in the microgrid. In mode-1, specified amount of real and reactive power are shared between the utility and the microgrid through the back-to-back converters. Mode-2 is invoked when the power that can be supplied by the distributed generators (DGs) in the microgrid reaches its maximum limit. In such a case, the rest of the power demand of the microgrid has to be supplied by the utility. An arrangement between DGs in the microgrid is proposed to achieve load sharing in both grid connected and islanded modes. The back-to-back converters also provide total frequency isolation between the utility and the microgrid. It is shown that the voltage or frequency fluctuation in the utility side has no impact on voltage or power in microgrid side. Proper relay-breaker operation coordination is proposed during fault along with the blocking of the back-to-back converters for seamless resynchronization. Both impedance and motor type loads are considered to verify the system stability. The impact of dc side voltage fluctuation of the DGs and DG tripping on power sharing is also investigated. The efficacy of the proposed control arrangement has been validated through simulation for various operating conditions. The model of the microgrid power system is simulated in PSCAD.**

***Index Terms*—Active and reactive power sharing, back-to-back converters, microgrid.**

I. Introduction

THE interconnection of distributed generators (DGs) to the utility grid through power electronic converters has raised concern about proper load sharing between different DGs and the grid. Microgrid can generally be viewed as a cluster of distributed generators connected to the main utility grid, usually through voltage-source-converter (VSC) based interfaces. Concerning the interfacing of a microgrid to the utility system, it is important to achieve a proper load sharing by the DGs. A load sharing with minimal communication is the best in the distribution level as the network is complex, can be reconfigured and span over a large area. The most common method is the use of droop characteristics. Parallel converters have been controlled to deliver desired real and reactive power to the system. The use of local signals as feedback to control the converters is desirable, since in a real system, the distance between the converters may make an inter-communication impractical. With this in mind, this paper proposes a configuration that is suitable for supplying electrical power of high quality to the microgrid, specifically when it is being supplied through controlled converters.

The real and reactive power sharing can be achieved by controlling two independent quantities—the frequency and the fundamental voltage magnitude [1]–[5]. The system stability during load sharing has been explored in [2] and [3]. Transient stability of power system with high penetration level of power electronics interfaced (converter connected) distributed generation is explored in [5]. While [6]–[8] explore the microgrid testing and control, [9] proposes a single-phase high-frequency ac (HFAC) microgrid as a solution towards integrating renewable energy sources in a distributed generation system. For a better performance of the DGs and more efficient power management system, it is important to achieve a control over the power flow between the grid and the microgrid. With a bidirectional control on the power flow, it is possible not only to specify exact amount of power supplied by the utility but also the fed back power from microgrid to utility during lesser power demand in the microgrid.

With number of DGs and loads connected over a wide span of the microgrid, isolation between the grid and the microgrid will always ensure a safe operation. Any voltage or frequency fluctuation in the utility side has direct impact on the load voltage and power oscillation in the microgrid side. For a safe operation of any sensitive load, it is not desirable to have any sudden change in the system voltage and frequency. The isolation between the grid and microgrid not only ensures safe operation of the microgrid load, it also prevents direct impact of microgrid load change or change in DG output voltage on the utility side.

Protection of the devices both in utility and microgrid sides during any fault is always a major concern [10]–[13]. Proper protection schemes in the distributed generation system ensure a reliable operation. Of the many schemes that have been proposed, [10] explores the effect of high DG penetration on protective device coordination and suggests an adaptive protection scheme as a solution to the problems. In [11], a method has been proposed for determining the coordination of the rate of change of frequency (ROCOF) and under/over-frequency relays for dis-

Manuscript received January 23, 2008; revised December 17, 2008. This work was supported by the Australian Research Council (ARC) through the ARC Discovery Grant DP 0774092. Paper no. TPWRS-00065-2008.

The authors are with the School of Engineering Systems, Queensland University of Technology, Brisbane, Qld 4001, Australia (e-mail: ritwik.majumder@student.qut.edu.au; a.ghosh@qut.edu.au; g.ledwich@qut.edu.au; f.zare@qut.edu.au).

Digital Object Identifier 10.1109/TPWRS.2009.2034666

tributed generation protection considering islanding detection and frequency-tripping requirements. The method is based on the concept of application region, which defines a region in the trigger time versus active power imbalance space where frequency-based relays can be adjusted to satisfy the anti-islanding and frequency-tripping requirements simultaneously.

In general, a microgrid is interfaced to the main power system by a fast semiconductor switch called the static switch (SS). It is essential to protect a microgrid in both the grid-connected and the islanded modes of operation against all faults. Inverter fault currents are limited by the ratings of the silicon devices to around 2 per unit rated current. Fault currents in islanded inverter based microgrids may not have adequate magnitudes to use traditional overcurrent protection techniques [12]. To overcome this problem, a reliable and fast fault detection method is proposed in [13].

The aim of this paper is to set up a power electronics interfaced microgrid containing distributed generators. A scheme for controlling parallel connected DGs for proper load sharing is proposed. The microgrid is connected to the utility with back-to-back converters. Bidirectional power flow control between the utility and microgrid is achieved by controlling both the converters. The back-to-back converters provide the much needed frequency and power quality isolation between the utility and the microgrid. A proper relay breaker co-ordination is proposed for protection during faults. The scheme not only ensures a quick and safe islanding at inception of the fault, but also a seamless resynchronization once the fault is cleared. The application of back-to-back converters in distributed generation would facilitate:

- controlled power flow between the microgrid and utility which can be used in case of any contractual arrangement;
- reliable power quality due to the isolation of the microgrid system from utility.

II. System Structure and Operation

A simple power system model with back to back converters, one microgrid load and two DG sources is shown in Fig. 1. A more complex case is considered in Section VIII. In Fig. 1, the real and reactive power drawn/supplied are denoted by P and Q, respectively. The back to back converters are connected to the microgrid at the point of common coupling (PCC) and to the utility grid at point A as shown in Fig. 1. Both the converters (VSC-1 and VSC-2) are supplied by a common dc bus capacitor with voltage of V_C. The converters can be blocked with their corresponding signal input BLK_1 and BLK_2. DG-1 and DG-2 are connected through voltage source converters to the microgrid. The output inductances of the DGs are indicated by inductance L_1 and L_2, respectively. The real and reactive powers supplied by the DGs are denoted by P_1, Q_1 and P_2, Q_2. While the real and reactive power demand from the load is denoted by P_L, Q_L. It is assumed that the microgrid is in distribution level with mostly resistive lines, whose resistances are denoted by R_{D1} and R_{D2}.

The utility supply is denoted by v_s and the feeder resistance and inductance are denoted, respectively, by R_s and L_s. The utility supplies P_G and Q_G to the back-to-back converters and the balance amounts $P_s - P_G$ and $Q_s - Q_G$ are supplied to

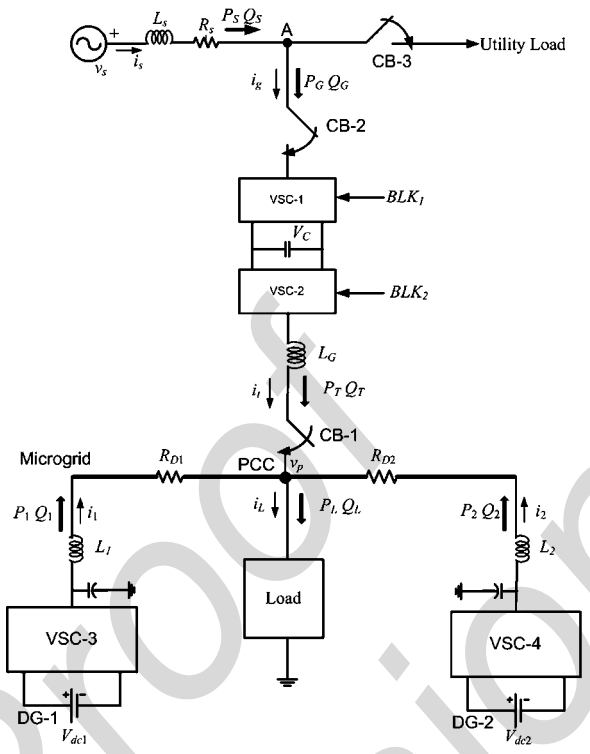

Fig. 1. Microgrid and utility system under consideration.

the utility load. The breakers CB-1 and CB-2 can isolate the microgrid from the utility supply. The power supplied from the utility side to microgrid at PCC is denoted by P_T, Q_T, where the differences $P_G - P_T$ and $Q_G - Q_T$ represent the loss and reactive power requirement of the back-to-back converter and their dc side capacitor.

The system can run in two different modes depending on the power requirement in the microgrid. In mode-1, a specified amount of real and reactive power can be supplied from the utility to the microgrid through the back-to-back converters. Rest of the load demand is supplied by the DGs. The power requirements are shared proportionally among the DGs based on their ratings. When the total power generation by the DGs is more than the load requirement, the excess power is fed back to the utility. This mode provides a smooth operation in a contractual arrangement, where the amount of power consumed from or delivered to the utility is pre-specified.

When the power requirement in the microgrid is more than the combined maximum available generation capacity of the DGs (e.g., when cloud reduces generation from PV), a pre-specified power flow from the utility to the microgrid may not be viable. The utility will then supply the remaining power requirement in the microgrid under mode-2 control, while the DGs are operated at maximum power mode. Once all the DGs reach their available power limits, the operation of the microgrid is changed from mode-1 to mode-2. While mode-1 provides a safe contractual agreement with the utility, mode-2 provides more reliable power supply and can handle large load and generation uncertainty. The rating requirement of the back to back converters will depend on the maximum power flowing through them. The maximum power flow will occur when

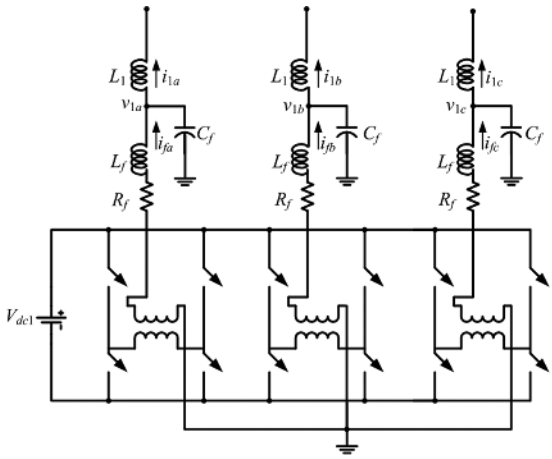

Fig. 2. Converter structure.

- the load demand in the microgrid is maximum and minimum power is generated by the DGs (power flow from utility to microgrid);
- maximum power is generated by DGs, while the load demand in the microgrid is minimum (power flow from microgrid to utility).

The rating issue has to be determined *a priori*. The microgrid cannot supply/absorb more power than the pre-specified maximum limit.

III. Converter Structure and Control

The converter structure for VSC-3 is shown in Fig. 2. DG-1 is assumed to be an ideal dc voltage source supplying a voltage of V_{dc1} to the VSC. The converter contains three H-bridges. The outputs of the H-bridges are connected to three single-phase transformers that are connected in wye for required isolation and voltage boosting [14]. The resistance R_f represents the switching and transformer losses. In this paper, an LCL filter structure is chosen to suppress the switching harmonics. This filter constitute of the leakage reactance of the transformers (L_f), the filter capacitor C_f is connected to the output of the transformers and L_1. Please note that L_1 also represents the output inductance of the DG source. The converter structure of DG-2 (VSC-4) is same as DG-1. The converters of the back-to-back converters have same structure but they are supplied by the common capacitor voltage V_C as shown in Fig. 1. It is to be noted that, while VSC-2 has an output inductance L_G (shown in Fig. 1), VSC-1 is directly connected to the point A without an output inductance. This implies that the voltage across the filter-capacitor (C_f in Fig. 2) of VSC-1 is the voltage of point A on the utility side. It is to be noted that the PSCAD simulations reported in this paper, all the converter are modeled in detail and no average linear model have been used.

All the converters are controlled in a similar way. The equivalent circuit of one phase of the converter is shown in Fig. 3. In this, $u \cdot V_{dc1}$ represents the converter output voltage, where u is the switching function that can take on values ± 1. The main aim of the converter control is to generate u.

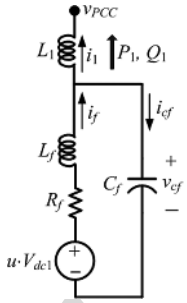

Fig. 3. Equivalent circuit of one phase of the converter.

From the circuit of Fig. 3, the state space description of the system can be given as

$$\dot{x} = Ax + B_1 u_c + B_2 v_{PCC} \tag{1}$$

where u_c is the continuous time control input, based on which the switching function u is determined. The discrete-time equivalent of (2) is

$$x(k+1) = Fx(k) + G_1 u_c(k) + G_2 v_{PCC}(k). \tag{2}$$

Let the output of the system given in (2) be v_{cf}. The reference for this voltage is given in terms of the magnitude of the rms voltage V_1^* and its angle δ_1^*. From these quantities, the instantaneous voltage references v_1^* for the three phases are generated. Neglecting the PCC voltage v_{PCC} assuming it to be a disturbance input, the input-output relationship of the system in (2) can be written as

$$\frac{v_{cf}(z)}{u_c(z)} = \frac{M(z^{-1})}{N(z^{-1})}. \tag{3}$$

The control is computed from

$$u_c(\mathrm{z}) = \frac{S(z^{-1})}{R(z^{-1})} \left\{ v_1^*(z) - v_{cf}(z) \right\}. \tag{4}$$

Then the closed-loop transfer function of the system is given by

$$\frac{v_{cf}(z)}{v_1^*(z)} = \frac{M(z^{-1})S(z^{-1})}{N(z^{-1})R(z^{-1}) + M(z^{-1})S(z^{-1})}. \tag{5}$$

The coefficients of the polynomials S and R can be chosen based on a pole placement strategy [15]. Once u_c is computed from (4), the switching function u can be generated as

$$\begin{aligned} &\text{If } u_c > h, \text{ then } u = +1 \\ &\text{elseif } u_c < -h, \text{ then } u = -1 \end{aligned} \tag{6}$$

where h is a small number.

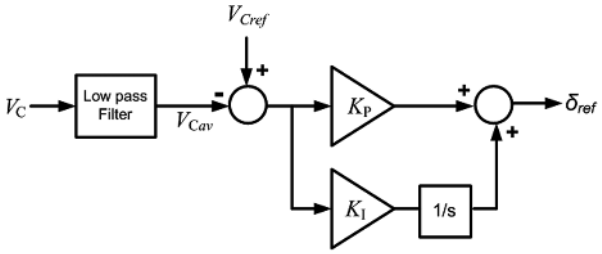

Fig. 4. Angle controller for VSC-1.

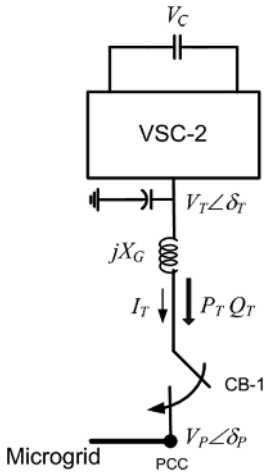

Fig. 5. Schematic diagram of VSC-2 connection to microgrid.

All the four VSCs are controlled using the above control strategy. Hence, all these controllers require their instantaneous reference voltages. These are discussed in the next two sections.

IV. Back-to-Back Converter Reference Generation

This section describe the reference generation for the back-to-back VSCs. Both the VSCs are supplied from a common capacitor of voltage V_C as shown in Fig. 1. Depending on the power requirement in the microgrid, there are two modes of operation as discussed in Section II. However the reference generation for VSC-1 is common for both these modes. This is discussed next.

A. VSC-1 Reference Generation

Reference angle for VSC-1 is generated as shown in Fig. 4. First the measured capacitor voltage V_C is passed through a low pass filter to obtain V_{Cav}. This is then compared with the reference capacitor voltage V_{Cref}. The error is fed to a PI controller to generate the reference angle δ_{ref}. VSC-1 reference voltage magnitude is kept constant, while angle is the output of the PI controller. The instantaneous voltages of the three phases are derived from them.

The two modes of VSC-2 reference generation are discussed next.

B. VSC-2 Reference Generation in Mode-1

VSC-2, which is connected with PCC through an output inductance L_G, controls the real and reactive power flow between the utility and the microgrid. Fig. 5 shows the schematic diagram of this part of the circuit, where the voltages and current are shown by their phasor values.

Let us assume that, in mode-1 the references for the real and reactive power be P_{Tref} and Q_{Tref}, respectively, and the VSC-2 output voltage be denoted by $V_T\angle\delta_T$ and the PCC voltage by $V_P\angle\delta_P$. Then the reference VSC-2 voltage magnitude and its can be calculated as

$$V_T = \frac{V_P^2 + Q_{Tref}X_G}{V_P\cos(\delta_T - \delta_P)} \tag{7}$$

$$\delta_T = \tan^{-1}\left(\frac{P_{Tref}X_G}{V_P^2 + Q_{Tref}X_G}\right) + \delta_P. \tag{8}$$

Depending on the real and reactive power demand, these references are calculated, based on which the instantaneous reference VSC-2 voltages for the three phases are computed. It is to be noted that, sign of the active and reactive power references are taken as negative when it is desired to supply the power from the microgrid to the utility side.

C. VSC-2 Reference Generation in Mode-2

In mode-2, the utility supplies any deficit in the power requirement through back-to-back converters while the DGs supply their maximum available power. Let the maximum rating of the back-to-back converters be given by P_{Tmax} and Q_{Tmax}. Then the voltage magnitude and angle reference of VSC-2 is generated as

$$\begin{aligned}\delta_T &= \delta_{T\max} - m_T \times (P_T - P_{T\max}) \\ V_T &= V_{T\max} - n_T \times (Q_T - Q_{T\max})\end{aligned} \tag{9}$$

where V_{Tmax} and δ_{Tmax} are the voltage magnitude and angle, respectively, when it is supplying the maximum load. The VSC-2 droop coefficient m_T and n_T are chosen such that the voltage regulation is within acceptable limit from maximum to minimum power supply.

V. Reference Generation for DG Sources

In this section, the reference generation for the DGs is presented. It is to be noted that the reference generations of the DGs are different from reference generation of the back-to-back converters. The control strategy for both the DGs is the same and hence only DG-1 reference generation is discussed here.

A. Mode-1

It is assumed that in mode-1 the utility supplies a part of the load demand through the back-to-back converters and rest of the power demand in the microgrid is supplied and regulated by the DGs. The output voltages of the converters are controlled to share this load proportional to the rating of the DGs. As the output impedance of the DG sources is inductive, the real and reactive power injection from the source to microgrid can be controlled by changing voltage magnitude and its angle. Fig. 6 shows the power flow from DG-1 to microgrid where the

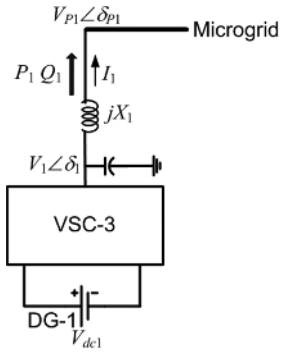

Fig. 6. Power flow from DG-1 to microgrid.

voltages and current are shown in rms values and the output impedance is denoted by jX_1.

The real and reactive power flow from DG to microgrid can be calculated as

$$P_1 = \frac{V_1 \times V_{P1}\sin(\delta_1 - \delta_{P1})}{X_1}$$
$$Q_1 = \frac{V_1^2 - V_1 \times V_{P1}\cos(\delta_1 - \delta_{P1})}{X_1}. \quad (10)$$

It is to be note that VSC-3 does not have any direct control over $V_{P1}\angle\delta_{P1}$. The output inductances of the DGs decouple the real and reactive power at the DG output. Hence from (10), it is clear that if the angle difference $(\delta_1 - \delta_{P1})$ is small, the real power can be controlled by controlling δ_1, while the reactive power can be controlled by controlling V_1. Thus the power requirement can be distributed among the DGs, similar to a conventional droop by dropping the voltage magnitude and angle as

$$\delta_1 = \delta_{1rated} - m_1 \times (P_1 - P_{1rated})$$
$$V_1 = V_{1rated} - n_1 \times (Q_1 - Q_{1rated}) \quad (11)$$

where V_{1rated} and δ_{1rated} are the rated voltage magnitude and angle, respectively, of DG-1, when it is supplying the load to its rated power levels of P_{1rated} and Q_{1rated}. The coefficients m_1 and n_1 respectively indicate the voltage angle drop vis-à-vis the real power output and the magnitude drop vis-à-vis the reactive power output. These values are chosen to meet the voltage regulation requirement in the microgrid. It is assumed that all the DGs are all converter based and so the output voltage angle can be changed instantaneously. The angle droop will be able to share the load without any drop in system frequency. In a microgrid with frequency droop, the variation of with normal load changes tends to be much higher than system grid frequency variation. In trying to correct this using low droop coefficient may lead to large variations in the frequency. Angle droop avoids this variation in frequency to some extent. A comparison of performance between angle and frequency droop is discussed in Appendix A.

To show the power sharing with angle droop, two DGs with a load is considered as shown in Fig. 7. The voltages and the

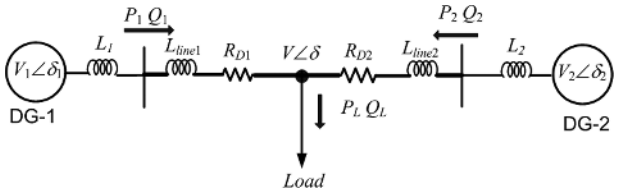

Fig. 7. Power sharing among the DGs.

power flow are indicated in the figure. Applying dc load flow with all the necessary assumptions, we get

$$\delta_1 - \delta = (X_1 + X_{L1})P_1$$
$$\delta_2 - \delta = (X_2 + X_{L2})P_2 \quad (12)$$

where $X_1 = \omega L_1/(V_1V)$, $X_2 = \omega L_2/(V_2V)$, $X_{L2} = \omega L_{Line2}/(V_2V)$, and $X_{L1} = \omega L_{Line1}/(V_1V)$. The angle droop equation of the DGs is given by

$$\delta_1 = \delta_{1rated} - m_1 \times (P_1 - P_{1rated})$$
$$\delta_2 = \delta_{2rated} - m_2 \times (P_2 - P_{2rated}). \quad (13)$$

The offset in the angle droop is taken such that when DG output power is zero, the DG source angle is zero. For this the rated droop angles are taken as $\delta_{1rated} = m_1P_{1rated}$ and $\delta_{2rated} = m_2P_{2rated}$. Then from (13), we get

$$\delta_1 - \delta_2 = -m_1P_1 + m_2P_2. \quad (14)$$

Similarly from (12), we get

$$\delta_1 - \delta_2 = (X_1 + X_{L1})P_1 - (X_2 + X_{L2})P_2. \quad (15)$$

Assuming the system to be lossless, we can find from Fig. 7 that $P_2 = P_L - P_1$ and substituting this (14) and (15), we get

$$(X_1 + X_{L1})P_1 - (X_2 + X_{L2})(P_L - P_1)$$
$$= -m_1P_1 + m_2(P_L - P_1)$$
$$\Rightarrow P_1 = \frac{X_2 + X_{L2} + m_2}{X_2 + X_{L2} + m_2 + X_1 + X_{L1} + m_1}P_L. \quad (16)$$

Similarly P_2 can be calculated as

$$P_2 = \frac{X_1 + X_{L1} + m_1}{X_2 + X_{L2} + m_2 + X_1 + X_{L1} + m_1}P_L. \quad (17)$$

From (16) and (17), the ratio of the output power is calculated as

$$\frac{P_1}{P_2} = \frac{X_2 + X_{L2} + m_2}{X_1 + X_{L1} + m_1}. \quad (18)$$

It is to be noted that the value of X_1 and X_2 are very small compared to the value of m_1 and m_2 (m_1 is ten times of X_1 in the example where $X_1 = 0.02595$ rad/MW). Moreover since the microgrid line is considered to be mainly resistive with low line inductance and the DG output inductance is much larger, we can write

$$m_1 \gg X_1 \gg X_{L1} \text{ and } m_2 \gg X_2 \gg X_{L2}.$$

Therefore, from (18), it is evident that the droop coefficients play the dominant role in the power sharing. As the droop coefficients are taken as inversely proportional to the DG rating, from (18), we can write

$$\frac{P_1}{P_2} \approx \frac{m_2}{m_1} = \frac{P_{1rated}}{P_{2rated}}. \tag{19}$$

The error is further reduced by taking the output inductance (L_1, L_2) of the DGs inversely proportional to power rating of the DGs. If the microgrid line is inductive in nature, and of high value, then network knowledge is needed to minimize the error by choosing the DG output inductance such that

$$\frac{X_1 + X_{line1}}{X_2 + X_{line2}} = \frac{P_{2rated}}{P_{1rated}}.$$

The system shown in Fig. 7 is a very simple example to show the power sharing. In a real system with number of DGs and loads in different locations, line impedances will have an impact on the load sharing. But for a microgrid within a small geographical area, the line inductances will never be very high. Moreover a high droop coefficient will always play a dominant role and share the power as desired with a very small deviation. The reactive power has been shared with the conventional voltage magnitude drop [1]–[4]. Since the converter output impedance is inductive, the change in output voltage angle does not have a significant effect on the reactive power sharing.

Thus DG-1 can supply the desired power if the output voltage of VSC-3 has magnitude and angle as given in (11). From the rms quantities the instantaneous reference voltages of the three phases are obtained. In a similar way, the instantaneous reference voltages for VSC-4 are also obtained. This method of load sharing is based only on local measurements and does not need intercommunication between the DGs. For the determination of the phase angles, a common reference is used. This can easily accomplished through a Global Positioning System (GPS) synchronizing signal. It is to be noted that the conventional frequency droop method can realize the real power sharing without such a GPS signal.

B. Mode-2

In mode-2, the DGs supply their maximum available power. The reference generation for the DGs in mode-2 is similar to the reference generation of VSC-2 of back-to-back converter in mode-1 as given in (7) and (8). Let us denote the available active power as P_{1avail}. Then based on this and the current rating of the DG, the reactive power availability Q_{1avail} of the DG can be determined. Based on these quantities, the voltage references as shown in Fig. 6 are calculated as

$$V_1 = \frac{V_{P1}^2 + Q_{1avail}X_1}{V_{P1}\cos(\delta_{P1} - \delta_P)} \tag{20}$$

$$\delta_1 = \tan^{-1}\left(\frac{P_{1avail}X_1}{V_{P1}^2 + Q_{1avail}X_1}\right) + \delta_{P1}. \tag{21}$$

The references for the other DGs are generated in a similar way.

VI. Relay and Circuit Breaker Coordination During Islanding and Resynchronization

The reference generations described in Section IV for DGs and back-to-back converters are totally independent of each other. In mode-1, once the desired value of real and reactive power flow through the back-to-back converters is set, the rest of the required power will automatically be shared amongst the DGs. In mode-2, the DGs supply their maximum available power while the extra the power requirement from utility is supplied through the back-to-back converter. When a DG reaches its maximum available power, it broadcasts it to VSC-2 control center. The mode change is initiated when all the DGs reach their available limits. Note that other than the broadcast signals, no other communication is needed between the back-to-back converters and the DGs, even during islanding and resynchronization. But proper relay breaker coordination, along with converter blocking, will be required to maintain the voltage of the dc capacitor during islanding and resynchronization. Fig. 8 shows the logic diagram used for this purpose, where *Trip_Signal* initiates the tripping of CB-2 (Fig. 1) and the signal BLK_1 blocks VSC-1. The same logic is also used for the tripping CB-1 and the blocking of VSC-2. The rate of rise of current i_g is monitored by the protection scheme. When it exceeds a threshold value in response to a fault in the utility grid, the output of the *Protection Scheme* (Fig. 8) becomes high. This output is used to set all the RS flip flops. The upper flip flop (F/F-1) generates the trip signal. This flip flop is reset by the *Fault_Clear* signal. The lower two flip flops, F/F-2 and F/F-3 generate BLK_1 and BLK_2 signals, respectively. The blocking deactivation is initiated when the fault is cleared and *Fault_Clear* signal is set high manually. The converter VSC-1 is deblocked by resetting F/F-2 when the breaker CB-2 is closed, as indicated by *Br_Status* signal. The AND gate insures that no false deblocking occurs till both these signals are high. VSC-2 is deblocked after VSC-1 is deblocked. This is why *Fault_Clear* signal is passed through a time delay circuit to generate the reset signal for F/F-3.

Fig. 9 shows the timing diagram of the breakers and converter blocking during islanding and resynchronization process. If a breaker is closed, the signal *Br_Status* is high and it goes low when the breaker opens. As evident from Fig. 8, the output of the *Protection Scheme* triggers the RS flip flops, which simultaneously generates both the trip and block signals. The block signals blocks both VSC-1 and VSC-2 simultaneously. Once the trip signals goes high, the breakers CB-1 and CB-2 open after a finite time delay (t_op) as indicated in Fig. 9. Unless the two VSCs are blocked, the dc capacitor voltage collapses due to the sudden increase in power requirement on the utility side. Also

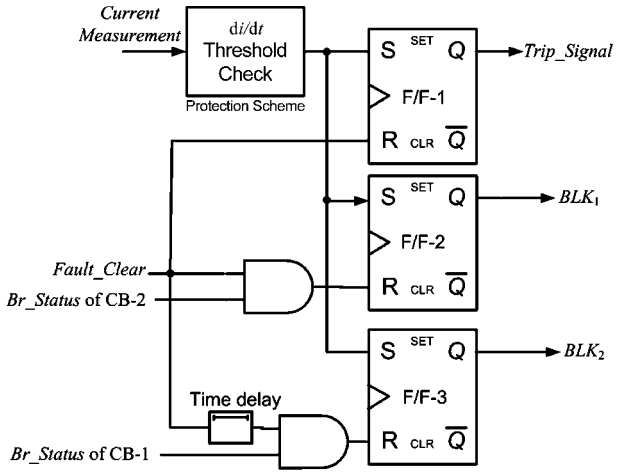

Fig. 8. Logic for breaker operation and converter blocking.

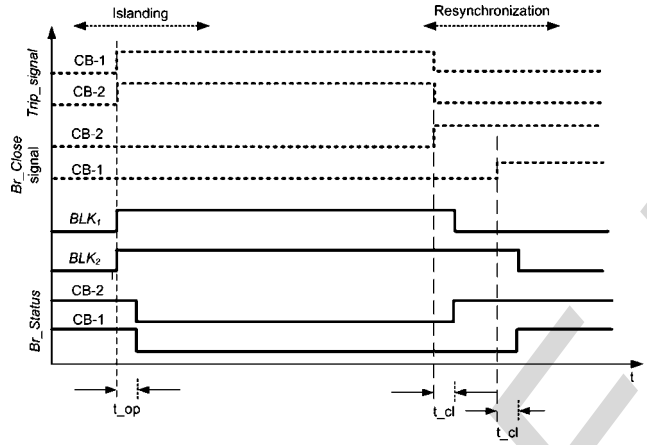

Fig. 9. Breakers and converter blocking timing diagram.

to prevent the angle reference δ_{ref} from diverging during the contingency, the angle controller of Fig. 4 is bypassed and the reference is held at the pre-fault value. Note that, once a breaker opens, the *Protection Scheme* output goes low causing the set input of the flip flops of Fig. 8 to become 0.

During islanding, breakers CB-1 and CB-2 are opened simultaneously. However during resynchronization, CB-2 is closed and VSC-1 is deblocked first connecting this to the utility. This will cause the dc capacitor voltage to rise taking a finite time depending on the capacitor voltage drop during islanding. Once the capacitor voltage settles to its reference value and the angle controller of Fig. 4 settles, CB-1 is closed and VSC-2 is deblocked.

Once the fault is cleared, *Fault_Clear* signal is set high manually. This signal is the same as *Br_Close* signal of CB-2. The *Fault_Clear* signal also resets *Trip_signal*, used both by CB-1 and CB-2. With a finite time delay (t_cl) from the initiation of *Br_Close* signal, CB-2 closes, making the *Br_Status* signal for CB-2 high. This resets F/F-2 and deactivates BLK_1 signal causing switching devices of VSC-1 to start conducting. As mentioned earlier and shown in Fig. 8, *Br_Close* signal for CB-1 is generated after a time delay from the *Fault_Clear* signal. Once this signal is generated, CB-1 closes after a time delay

TABLE I
SYSTEM AND CONTROLLER PARAMETERS

System Quantities	Values
Systems frequency	50 Hz
Source voltage (V_s)	11 kV rms (L-L)
Feeder impedance	R_s = 3.025 Ω, L_s = 57.75 mH
Load	
Impedance (Balanced)	R_L = 100.0 Ω, L_L = 300.0 mH
or	
Induction motor	Rated 40 hp, 11 kV rms (L-L)
DGs and VSCs	
DC voltage (V_{dc1}, V_{dc2})	3.5 kV
Transformer rating	3 kV/11 kV, 0.5 MVA, 2.5% reactance (L_f)
VSC losses (R_f)	1.5 Ω
Filter capacitance (C_f)	50 μF
Inductances (L_1, L_2)	20 mH and 16.0 mH
Inductances (L_G)	28.86 mH
Hysteresis constant (h)	10^{-5}
Angle Controller	
Proportional gain (K_P)	– 0.2
Integral gain (K_I)	– 5.0
Droop Coefficients	
Power–angle	
m_1	0.3 rad/MW
m_2	0.24 rad/MW
Voltage–Q	
n_1	0.15 kV/MVAr
n_2	0.12 Kv/MVAr

t_cl. This then resets F/F-3 and VSC-2 starts conducting. To even further safeguard the dc capacitor voltage, the power flow reference for VSC-2 is switched to zero during islanding and brought back to its previous value after resynchronization. This step by step process ensures a seamless resynchronization.

VII. SIMULATION STUDIES

Simulation studies are carried out in PSCAD/EMTDC (version 4.2). Different configurations of load and its sharing are considered. The DGs are considered as inertia-less dc source supplied through a VSC. The system data are given in Table I. The droop coefficients are chosen such that both active and reactive powers of the load are divided in a ratio of 1:1.25 between DG-1 and DG-2. Some of the simulation results to indicate the accuracy of the proposed control are listed in Table II, given in Appendix B.

A. Case-1: Load Sharing of the DGs With Utility

If the power requirement of the load in microgrid is more than the power generated by the DGs, the balance power is supplied by the utility through the back-to-back converters. The desired power flow the utility to the microgrid is controlled by (7) and (8), while droop (10) controls the sharing of the remaining power. It is desired that 50% of the load is supplied by the utility and rest of the load is shared by DG-1 and DG-2. The impedance load of Table I is considered for this case. Fig. 10 shows the real and reactive power sharing between utility and the DGs. Fig. 11(a) shows the phase-a reference and output voltage, whereas three-phase voltage tracking error is shown in Fig. 11(b). It can be seen that the tracking error is less than 0.2%. Fig. 12 shows the capacitor voltage and the output of the angle controller. At 0.1 s, the impedance of the load is halved and at 0.35 s, it is changed back to its nominal value. It can be seen

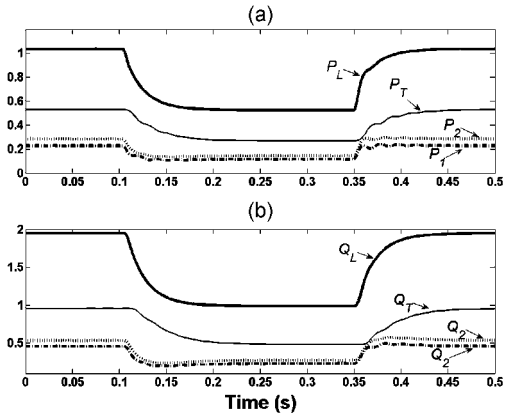

Fig. 10. Real and reactive power sharing for Case-1. (a) Real power sharing (MW). (b) Reactive power sharing (MVAr).

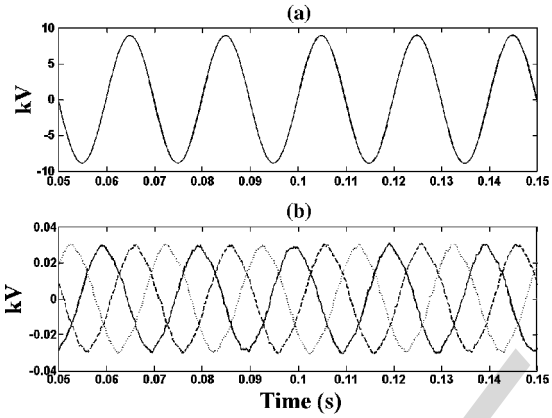

Fig. 11. Voltage tracking of DG-1 Case-1. (a) Phase-a references and output voltages of DG-1. (b) Voltage tracking errors of the three phases of DG-1.

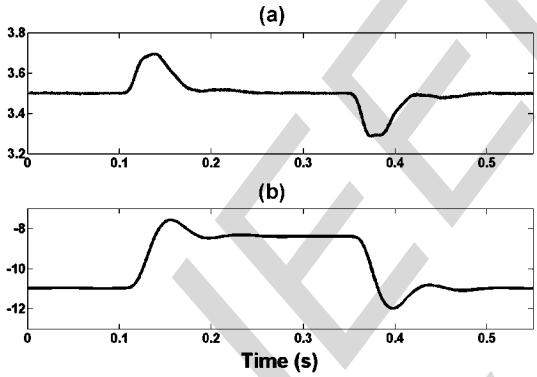

Fig. 12. Capacitor voltage and angle controller output for Case-1. (a) Capacitor voltage (kV). (b) Angle controller output (degree).

that the system goes through minimal transient and reaches its steady state within five cycles (100 ms) for both the transients.

B. Case-2: Change in Power Supply From Utility

If the power flow from the utility to the microgrid is changed by changing the power flow references for VSC-2, the extra power requirement is automatically picked up by the DGs. Fig. 13 shows the real and reactive power sharing, where at 0.1 s the power flow from the utility is changed to 20% of the total load from the initial value of 50% as considered in

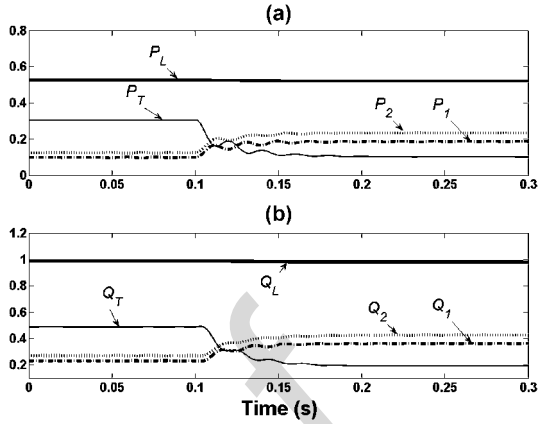

Fig. 13. Real and reactive power sharing for Case-2. (a) Real power sharing (MW). (b) Reactive power sharing (MVAr).

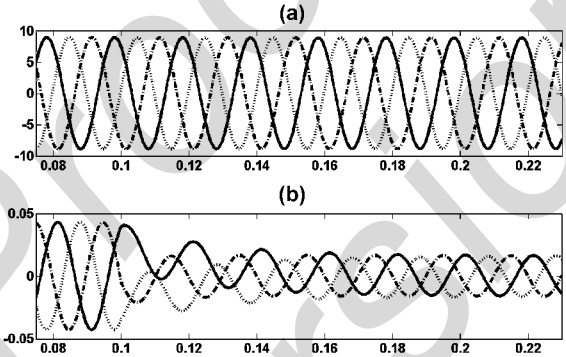

Fig. 14. Three-phase PCC voltage and injected current for Case-2. (a) Three-phase PCC voltage (kV). (b) Three-phase current injected at PCC by back-to-back inverter (kA).

Case-1. It can be seen that the DGs pick up the balance load demand and share it proportionally as desired. The unchanged real and reactive load power during the change over proves the efficacy of the controller for smooth transition. Fig. 14 shows the PCC voltage and change in current injection at PCC from utility. It can be seen that the PCC voltage remained balanced and transient-free, while the injected currents reach steady state within four cycles.

C. Case-3: Power Supply From Microgrid to Utility

When the power generation of the DGs is more than the power requirement of the load, excess power can be fed back to the utility through the back-to-back converters. It is desired that the utility supplies 50% of the microgrid load initially. At 0.1 s, however, the same amount of power is fed back to the utility by changing the sign of the power flow reference for the back-to-back converters. The DG output increases automatically to supply the total load power and power to the utility, as evident from Fig. 15.

Fig. 16(a) shows the phase-a voltage at PCC and phase-a current injected from the utility to the microgrid, where current is scaled up 30 times. The change in the power flow direction is indicated by the sudden change in phase of the injected current phase at 0.1 s, vis-à-vis that of the voltage. Fig. 16(b) shows the three-phase current injected by the utility to the microgrid. It reaches steady state within three cycles. Apart from the phase

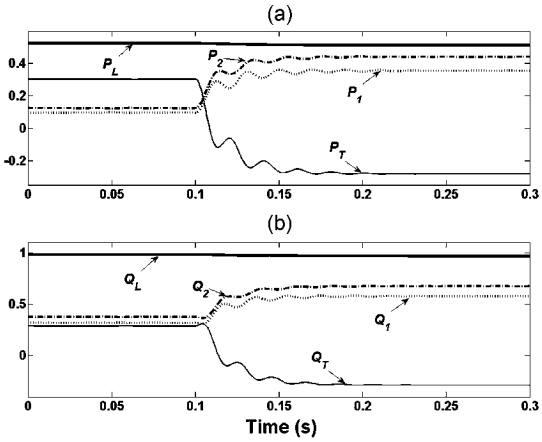

Fig. 15. Real and reactive power sharing during power reversal (Case-3). (a) Real power sharing (MW). (b) Reactive power sharing (MVAr).

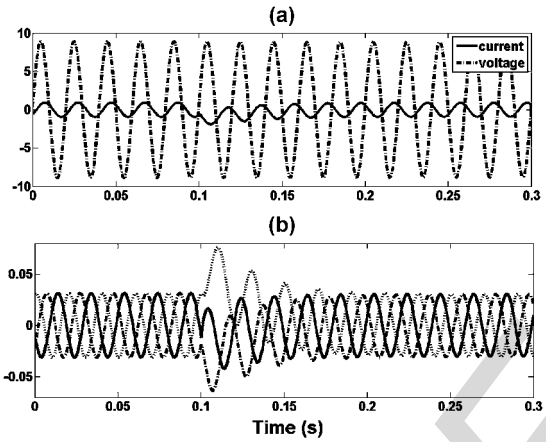

Fig. 16. PCC voltage and injected current for Case-3. (a) Phase-a PCC voltage (kV) and phase-a current from utility to microgrid (kA), scaled up 30 times. (b) Three-phase current injected from utility to microgrid (kA).

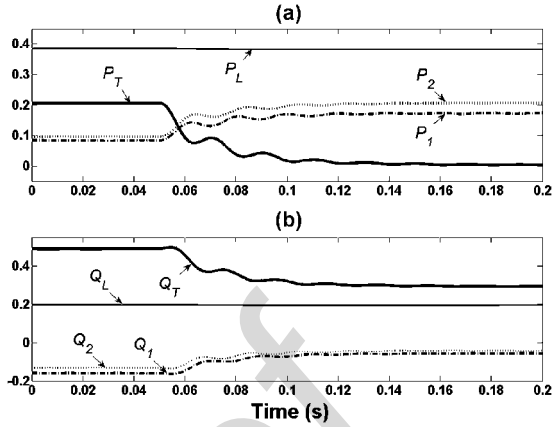

Fig. 17. Real and reactive power sharing with motor load (Case-4). (a) Real power sharing (MV). (b) Reactive power sharing (MVAr).

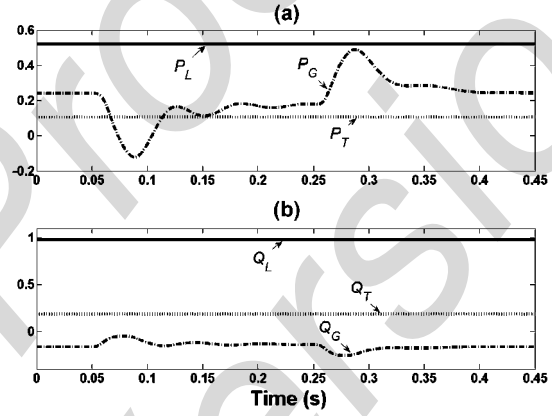

Fig. 18. Real and reactive power during frequency fluctuation (Case-5). (a) Real power (MW). (b) Reactive power (MVAr).

reversal, the magnitude of the currents remain the same, indicating that the same amount of power flow is taking place, albeit in the opposite direction.

D. Case-4: Load Sharing With Motor Load

In this section, load sharing with the induction motor load, given in Table I, is investigated. An impedance load is an infinite sink as it can absorb any change in the instantaneous real and reactive power. However an inertial load such as motor is not capable of that. Thus any sudden big change in the terminal voltage results in large oscillation in the real and reactive power. At the beginning it is assumed that the utility supplies 0.2 MW of real power and 0.5 MVAr of reactive power to the microgrid. Then at 0.05 s, the power reference is changed such that the utility supplies 0.3 MVAR of reactive power and no real power. The power sharing results for this case are shown in Fig. 17.

E. Case-5: Change in Utility Voltage and Frequency

One of the major advantages of the back-to-back converter connection is that it can provide isolation between the utility and the microgrid, both for voltage and frequency fluctuations. Fig. 18 shows the system response for frequency fluctuation in the utility side from 0.05 s to 0.25 s. At 0.05 s, the utility frequency dropped by 0.5%, and at 0.25 s, it comes back to its initial value of 50 Hz. The real and reactive power injections from utility to VSC-1 are shown as $P_{\rm G}$ and $Q_{\rm G}$, respectively. It can be seen that while $P_{\rm G}$ and $Q_{\rm G}$ fluctuate, the load power (P_L, Q_L) and the injected power to the microgrid (P_T, Q_T) remain constant.

With the system operating in steady state, a 50% balanced sag in the source voltage occurs in 0.1 s. The sag is removed after 0.5 s. Fig. 19 shows the power and the reactive power during this condition. It can be seen that the load power (P_L, Q_L) and the injected power to the microgrid (P_T, Q_T) remain almost undisturbed. The real power drawn from the grid (P_G), barring transients at the inception and removal of the sag, is maintained at the steady state level in order to supply power to the microgrid. The reactive power (Q_G) however reverses sign as the utility voltage drop causing it to absorb reactive power. During the sag, the dc capacitor supplies reactive power to the utility. The dc capacitor voltage and the output of the angle controller are shown in Fig. 20. It can be seen that while the dc capacitor voltage is maintained at its pre-specified value, the angle drops in sympathy with the source voltage drop to maintain the

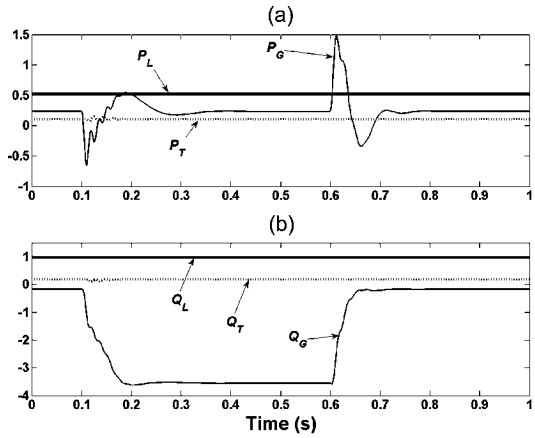

Fig. 19. Real and reactive power during voltage sag (Case-5). (a) Real power (MW) during voltage sag. (b) Reactive power (MVAr) during voltage sag.

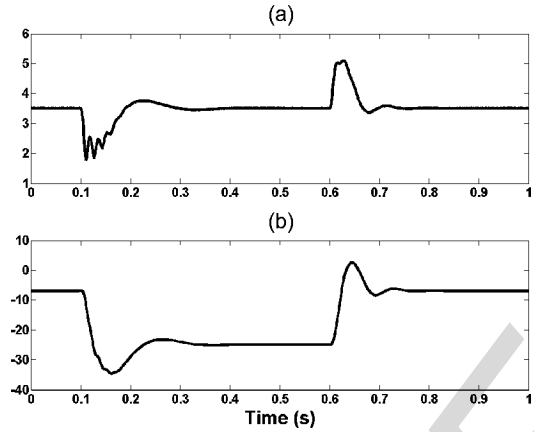

Fig. 20. DC capacitor voltage and angle controller output during voltage sag. (a) DC capacitor voltage (kV). (b) Angle controller output (degree).

injected power constant. The angle returns to its pre-sag value once the sag is removed.

F. Case-6: Islanding and Resynchronization

In this section the system response during a fault in the utility is investigated. Let us assume that a single-line to ground fault occurs at point F, which is half way between the utility source and point A, as shown in Fig. 21. As the fault occurs, the trip signal for the breakers CB-1 and CB-2 are initiated by the protection scheme which measure the rate of rise of current i_g. But breakers need a finite time to physically open the contact. During this time, the back to back converters start feeding the fault as shown by $P_{\rm G}, Q_{\rm G}$ in Fig. 21, which will result in the collapse of the capacitor voltage $V_{\rm C}$. As explained in Section VI, the coordination of breaker tripping and VSC blocking is required to avoid the voltage collapse.

With the system operating in steady state, the single-line to ground fault in phase-a occurs at 0.05 s and the fault is cleared at 0.1 s. The resynchronization process starts at 0.25 s when the *Br_Close* signal of CB-2 is generated. Subsequently, at 0.35 s, the *Br-Close* signal of CB-1 is generated. The dc capacitor voltage and the angle controller output are shown in Fig. 22 in which the angle controller output is kept constant to its pre-fault

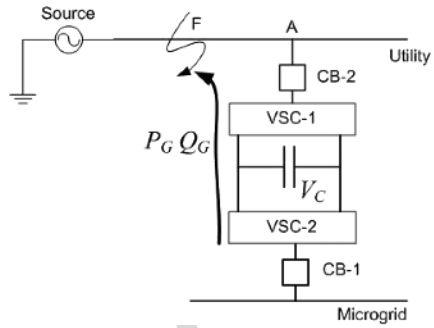

Fig. 21. Location of the single-line to ground fault.

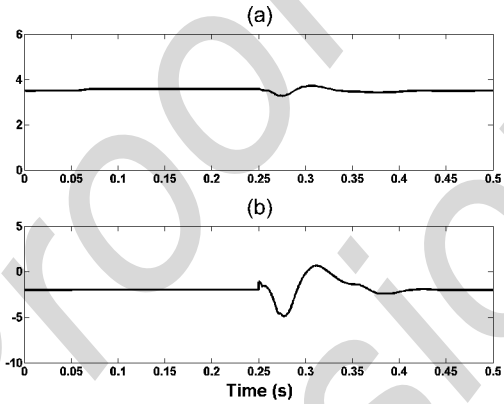

Fig. 22. DC capacitor voltage and angle controller output during islanding and resynchronization (Case-6). (a) Capacitor voltage (kV). (b) Angle controller output (degree).

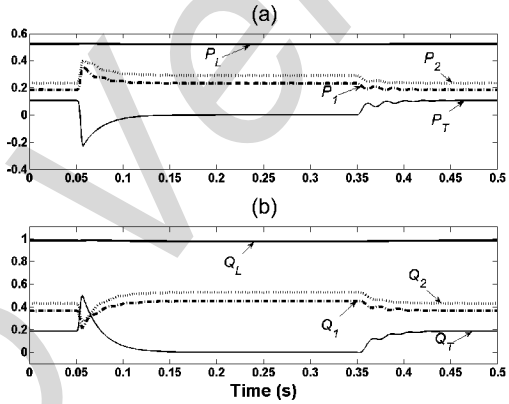

Fig. 23. Real and reactive power during islanding and resynchronization (Case-6). (a) Real power sharing (MW). (b) Reactive power sharing (MVAr).

value between 0.05 s to 0.25 s. Fig. 23 shows real and reactive power sharing, which are in accordance to the desired objective to keep microgrid load power constant.

G. Case-7: Variable Power Supply From Utility

In cases presented above, it has been assumed that the system is running in mode-1 where DGs can supply the balance of the load requirement once the pre-specified amount of power is drawn from the utility. The following example shows the switch from mode-1 to mode-2 when the maximum available power that can be supplied by the DGs is reached. Initially, the microgrid is running in mode 1. At 0.1 s, the input power from

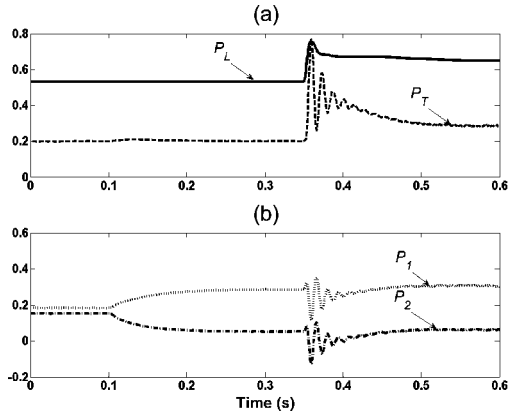

Fig. 24. Real power sharing during power limit and mode change (Case-7). (a) Real power demand from load and supply through utility (MW). (b) Real power sharing by the DGs (MW).

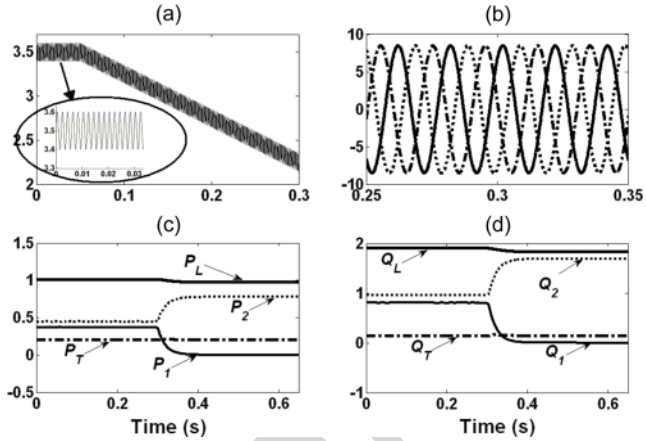

Fig. 25. DC voltage fluctuation in DG-1 and its tripping (Case-8). (a) DC voltage fluctuation (kV). (b) v_{p1} (kV). (c) Real power sharing (MW). (d) Reactive power sharing (MVAr).

DG-1 (P_{1avail}) suddenly reduces to 60 KW. DG-2 then supplies the shortfall as can be seen in Fig. 24. The load power and that supplied by the utility remain unchanged. Subsequent to this, suddenly the load changes at 0.35 s in which the power demand in the microgrid increases from 0.53 MW to 0.64 MW. However, the maximum power that can be supplied by DG-2 is set at 300 kW. This implies that both the DGs together can supply 360 KW. Moreover, the utility grid was supplying 200 kW before this event. Therefore an additional 80 KW of power is required from the utility grid and hence a mode change is inevitable. This mode change is initiated with VSC-2 droop gains of $m_T = 0.03$ rad/MW and $n_T = 0.02$ kV/MVAr. The results are also shown in Fig. 24. It can be seen that there is no appreciable overshoot in the active powers supplied by the DGs. The utility power (P_T) rises sharply in order to supply the load demand. The system settles in five cycles.

H. Case-8: DC Voltage Fluctuation and Loss of a DG

Photovoltaic (PV) cells are the most common form of converter interfaced DGs. The power output from these cells may vary during the day and may also have fluctuations depending on the atmospheric conditions. However as long as the dc voltage remains above a threshold, the converter tracks the output voltage reference. If the voltage falls below this threshold, the converter is switched off and the utility and the other DGs will have to share the microgrid load. To prove this point, a simulation is carried out in which it is assumed that DG-2 is capable of supplying the excess load demand, while the utility supplies the pre-specified amount of power in mode-1. If this is not possible, a switch to mode-2 will be necessary, which is not shown here.

The simulation results for this case are shown in Fig. 25. The dc voltage of DG-1 has a sinusoidal fluctuation of 3% and at 0.05 s, it starts ramping down as in Fig. 25(a). The 500-Hz fluctuation is shown in the inset. At 0.3 s, when the dc voltage falls below 2.25 kV, this DG is isolated from the system. Since the other DG picks up the load, any appreciable drop in v_{p1} (Fig. 6) does not occur as evident from Fig. 25(b). Fig. 25(c) and (d) shows the real and reactive powers, respectively. It can be seen that there is a slight drop in the load power indicating a slight microgrid voltage drop. However the utility power remains unchanged and that supplied by DG-2 increases.

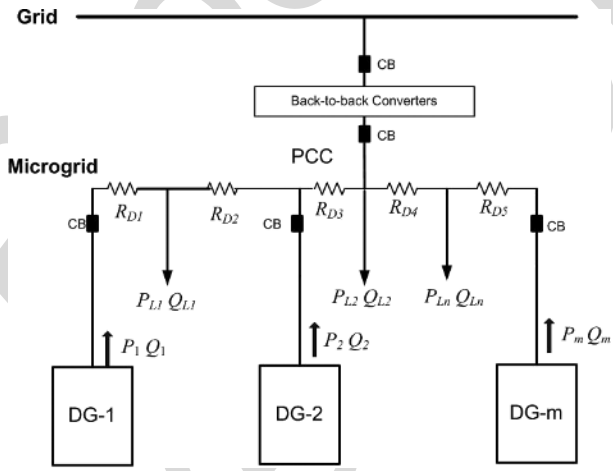

Fig. 26. Microgrid structure with large number of DGs and loads.

VIII. Microgrid Containing Multiple DGs

In the studies presented so far, it has been assumed that only two DGs and a load are connected to the microgrid. In general, however, there might be several DGs and loads connected to it, as shown in Fig. 25. It is assumed that there are a total number of n loads and m DGs. The total active and reactive powers consumed by the loads are given by

$$\begin{aligned} P_L &= P_{L1} + P_{L2} + \cdots + P_{Ln} \\ Q_L &= Q_{L1} + Q_{L2} + \cdots + Q_{Ln}. \end{aligned} \tag{22}$$

The required power will be shared by DGs depending on their rating, given by

$$\begin{aligned} m_1 \times P_{1rated} &= m_2 \times P_{2rated} = \cdots = m_m \times P_{mrated} \\ n_1 \times Q_{1rated} &= n_2 \times Q_{2rated} = \cdots = n_m \times Q_{mrated}. \end{aligned} \tag{23}$$

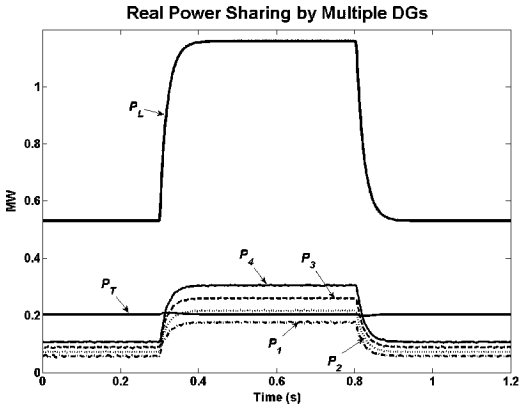

Fig. 27. Real power sharing with four DGs.

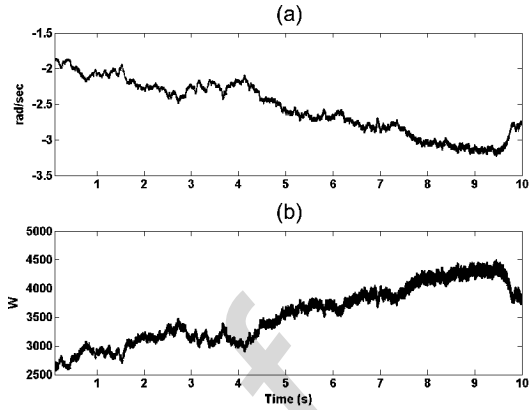

Fig. 28. Frequency deviation with frequency droop control. (a) Frequency deviation with frequency droop (DG-2). (b) Power output with frequency droop (DG-2).

However, like any droop method, the different line impedance between the load connection points, throughout the microgrid will have slight impact on the load sharing. The reference generation for the DGs will remain the same as before.

To validate a proper load sharing with multiple DGs, two more DGs are connected to the microgrid. The DG parameters, output impedance, converter structure and controller are the same as those used for DG-1 and DG-2. The droop coefficients for the four DGs are chosen such that they share both real and reactive power in the ratio of DG-1: DG-2: DG-3: DG-4 equal to 1:1.25:1.55:1.72. The load is also distributed in three different places to achieve a microgrid structure similar as shown in Fig. 26 with $m = 4$ and $n = 3$. Fig. 27 shows the real power sharing, where the load power demand is doubled at 0.3 s, and brought back to initial value at 0.8 s. It is evident from the figure that a proper load sharing occurs in the desired ratio.

IX. Conclusions

In this paper, a load sharing and power flow control technique is proposed for a utility connected microgrid. The utility distribution system is connected to the microgrid through a set of back-to-back converters. In mode-1, the real and reactive power flow between utility and microgrid can be controlled by setting the specified reference power flow for back-to-back converters module. Rest of the power requirement in the microgrid is shared by the DGs proportional to their rating. In case of high power demand in the microgrid, the DGs supply their maximum power, while rest of the power demand is supplied by utility through back-to-back converters (mode-2). A broadcast signal can be used by the DGs to indicate their mode change. However only locally measured data are used by the DGs and no communication is needed for the load sharing. The utility and microgrid are totally isolated, and hence, the voltage or frequency fluctuations in the utility side do not affect the microgrid loads. Proper switching of the breaker and other power electronics switches has been proposed during islanding and resynchronization process. The efficacy of the controller and system stability is investigated in different operating situation with various types of loads.

Appendix A

To show the relative differences between the angle and frequency droop controllers, we have chosen a simple system as shown in Fig. 7. The frequency droop controller is given by [1]–[4]

$$\omega = \omega_{ref} - m(P - P_{ref}). \tag{A1}$$

The output impedances of the two sources are chosen in a ratio of 1:1.33 and the powers are also chosen in the ratio of 1.33:1. No reactive power droop has been used and the voltage magnitudes are held constant. Both frequency and angle droop controller gains are chosen at 50% of their respective marginal stability points. The VSCs and DGs ratings for both cases are assumed to be identical.

The load in Fig. 7 is assumed to be resistive. To represent random changes of customer load, the conductance is chosen as the integral of a Gaussian white noise source with zero mean and standard deviation of 0.01 Mho. The output inductances of the two converters are 25 mH and 18.8 mH. The impedance of line 1 is $0.25 + j1.6$ while impedance of line 2 is $0.1 + j0.95$. Fig. 28 shows the steady state frequency variation and power output of DG-2 with frequency droop controller, while those with angle droop controller are shown in Fig. 29. It can be seen that with the frequency droop controller, the relation between frequency deviation and power output obeys (A1). A similar relationship also exists between angle and output power with angle droop control (11), which is not shown here. The variation in frequency with the frequency droop controller is significantly higher than that with the angle droop controller. The standard deviation for the window shown is 0.153 rad/s with the frequency droop controller, while it is 0.0011 rad/s with the angle droop controller. It can also be seen that the mean frequency deviation is much larger in case of frequency droop than in angle droop. This demonstrates that the angle droop controller generates a substantially smaller frequency variation than the conventional frequency droop controller.

The output power and current of DG-1 is shown in Fig. 30 for both frequency and angle droop controllers. Since the output currents in this figure are essentially the same and the DGs are

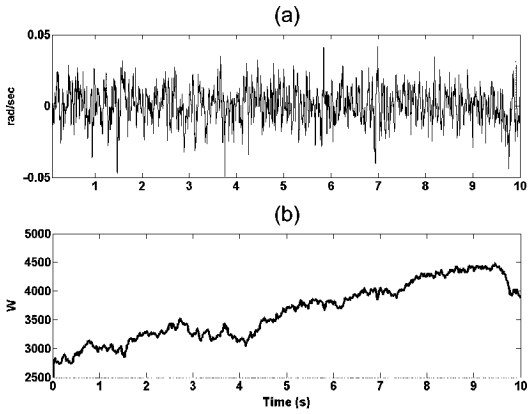

Fig. 29. Frequency deviation with angle droop control. (a) Frequency deviation with angle droop (DG-2). (b) Power output with angle droop (DG-2).

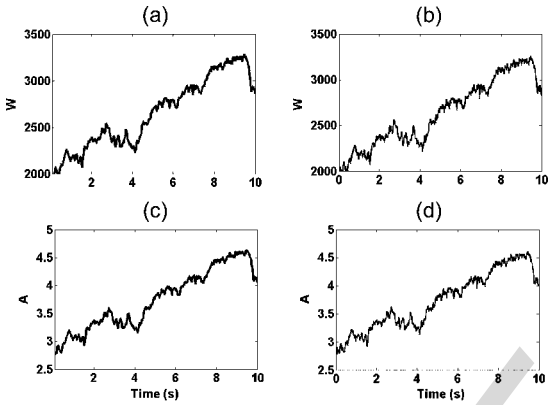

Fig. 30. Output power and current of DG-1 for both droop control methods.

operated at same constant voltage of 1000 V in both cases, the required power of the VSCs is also the same. As the load is not modeled as frequency dependant, the total power being supplied under both control schemes is also closely matched, as evident from Fig. 30. The switching frequency in both the cases is the same. Thus the converter requirements are the same in both the control schemes. For a given frequency error, there will be a finite (proportional) response from the frequency droop controller. In the same situation, the angle droop controller output will continue to ramp until the frequency error is corrected. In normal operation, this will give a superior transient correction term in the angle droop control output, while the steady state power matches the load demand in both control schemes.

APPENDIX B

Some of the simulation results to indicate the accuracy of the proposed control are listed in Table II.

TABLE II
NUMERICAL RESULTS

Case-1		Power	Initial value	Intermediate value	Final value
Section VII.A Load Sharing of the DGs with Utility	Fig. 9	P_1	0.24 MW	0.119 MW	0.24MW
		P_2	0.3 MW	0.15 MW	0.3
		P_T	0.56 MW	0.275 MW	0.56 MW
		P_L	1.1 MW	0.55 MW	1.1 MW
		Q_1	0.45 MVAr	0.23 MVAr	0.45 MVAr
		Q_2	0.55 MVAr	0.272 MVAr	0.55 MVAr
		Q_T	0.98 MVAr	0.5 MVAr	0.98 MVAr
		Q_L	1.98 MVAr	1.0 MVAr	1.98 MVAr
	Fig. 10		Initial value	Intermediate value	Final value
		Capacitor Voltage (kV)	3.501 kV	3.50 kV	3.501 kV
		Angle Controller Output (degree)	-10.8	-8.4	-10.8
Case-2		Power	Initial value		Final value
Section VII.B Change in Power	Fig. 11	P_1	0.131 MW		0.2058 MW
		P_2	0.169 MW		0.2575 MW
		P_T	0.271 MW		0.117 MW
		P_L	0.55 MW		0.55 MW
Supply from Utility		Q_1	0.221 MVAr		0.35 MVAr
		Q_2	0.278 MVAr		0.439 MVAr
		Q_T	0.49 MVAr		0.2 MVAr
		Q_L	0.99 MVAr		0.99 MVAr
Case-3		Power	Initial value		Final value
Section VII.C Power supply from Micro-grid to Utility	Fig. 13	P_1	0.131 MW		0.369 MW
		P_2	0.169 MW		0.461 MW
		P_T	0.281 MW		-0.281 MW
		P_L	0.55 MW		0.55 MW
		Q_1	0.332 MVAr		0.55 MVAr
		Q_2	0.416 MVAr		0.69 MVAr
		Q_T	0.25 MVAr		-0.25 MVAr
		Q_L	0.99 MVAr		0.99 MVAr
Case-Multiple DGs		Power	Initial value	Intermediate value	Final value
Section VIII Real Power Sharing with Four DGs	Fig. 25	P_1	0.0616 MW	0.161 MW	0.0616 MW
		P_2	0.077 MW	0.202 MW	0.077 MW
		P_3	0.0954 MW	0.25 MW	0.0954 MW
		P_4	0.1059	0.277	0.1059
		P_T	0.21 MW	0 21MW	0.21 MW
		P_L	0.55 MW	1.1 MW	0.55 MW

REFERENCES

[1] F. Katiraei and M. R. Iravani, "Power management strategies for a microgrid with multiple distributed generation units," *IEEE Trans. Power Syst.*, vol. 21, no. 4, pp. 1821–1831, Nov. 2006.

[2] M. Reza, D. Sudarmadi, F. A. Viawan, W. L. Kling, and L. Van Der Sluis, "Dynamic stability of power systems with power electronic interfaced DG," in *Proc. Power Systems Conf. Expo. (PSCE'06)*, 2006, pp. 1423–1428.

[3] J. M. Guerrero, L. G. de Vicuna, J. Matas, M. Castilla, and J. Miret, "A wireless controller to enhance dynamic performance of parallel inverters in distributed generation systems," *IEEE Trans. Power Electron.*, vol. 19, no. 5, pp. 1205–1213, Sep. 2004.

[4] M. C. Chandorkar, D. M. Divan, and R. Adapa, "Control of parallel connected inverters in standalone ac supply systems," *IEEE Trans. Ind. Appl.*, vol. 29, no. 1, pp. 136–143, Jan./Feb. 1993.

[5] J. G. Slootweg and W. L. Kling, "Impacts of distributed generation on power system transient stability," in *Proc. IEEE Power Eng. Soc. Summer Meeting*, 2002, vol. 2, pp. 862–867.

[6] L. Yunwei, D. M. Vilathgamuwa, and C. L. Poh, "Design, analysis, and real-time testing of a controller for multibus microgrid system," *IEEE Trans. Power Electron.*, vol. 19, no. 5, pp. 1195–1204, Sep. 2004.

[7] A. L. Dimeas and N. D. Hatziargyriou, "Operation of a multiagent system for microgrid control," *IEEE Trans. Power Syst.*, vol. 20, no. 3, pp. 1447–1455, Aug. 2005.
[8] J. A. P. Lopez, C. L. Moreira, and A. G. Madureira, "Defining control strategies for microgrid islanded operation," *IEEE Trans. Power Syst.*, vol. 21, no. 2, pp. 916–924, May 2006.
[9] S. Chakroborty, M. D. Weiss, and M. G. Simoes, "Distributed intelligent energy management system for a single-phase high-frequency ac microgrid," *IEEE Trans. Ind. Electron.*, vol. 54, no. 1, pp. 97–109, Feb. 2007.
[10] S. M. Brahma and A. A. Girgis, "Development of adaptive protection scheme for distribution systems with high penetration of distributed generation," *IEEE Trans. Power Del.*, vol. 19, no. 1, pp. 56–63, Jan. 2004.
[11] J. C. M. Vieira, W. Freitas, W. Xu, and A. Morelato, "Efficient coordination of ROCOF and frequency relays for distributed generation protection by using the application region," *IEEE Trans. Power Del.*, vol. 21, no. 4, pp. 1878–1884, Oct. 2006.
[12] H. Nikkhajoei and R. H. Lasseter, "Microgrid protection," in *Proc. IEEE Power Eng. Soc. General Meeting*, Tampa, FL, 2007.
[13] H. Al-Nasseri, M. A. Redfern, and R. O'Gorman, "Protecting microgrid systems containing solid-state converter generation," in *Proc. Int. Conf. Future Power Systems*, 2005.
[14] A. Ghosh and A. Joshi, "A new approach to load balancing and power factor correction in power distribution system," *IEEE Trans. Power Del.*, vol. 15, no. 1, pp. 417–422, Jan. 2000.
[15] A. Ghosh, "Performance study of two different compensating devices in a custom power park," *Proc. Inst. Elect. Eng., Gen., Transm., Distrib.*, vol. 152, no. 4, pp. 521–528, Jul. 2005.

Ritwik Majumder (S'07) received the B.E. degree in electrical engineering from Bengal Engineering College (Deemed University), Howrah, India, in 2001 and the M.Sc. (Engg.) degree from Indian Institute of Science, Bangalore, India, in 2004. Since June 2007, he has been pursuing the Ph.D. degree at Queensland University of Technology, Brisbane, Australia.

From July 2004 to November 2004, he was with Tata Motor Engineering Research Centre, Jamshedpur, India. From November, 2004 to January 2006, he was with Siemens Automotive India and from January 2006 to May 2007, he was with ABB Corporate Research Centre, Bangalore, India. His interests are in power systems dynamics, distributed generation, and power electronics applications.

Arindam Ghosh (S'80–M'83–SM'93–F'06) received the Ph.D. degree in electrical engineering from the University of Calgary, Calgary, AB, Canada, in 1983.

He is a Professor of power engineering at Queensland University of Technology (QUT), Brisbane, Australia. Prior to joining the QUT in 2006, he was with the Department of Electrical Engineering at IIT Kanpur, India, for 21 years. His interests are in control of power systems and power electronic devices.

Dr. Ghosh is a fellow of the Indian National Academy of Engineering (INAE).

Gerard Ledwich (M'73–SM'92) received the Ph.D. degree in electrical engineering from the University of Newcastle, Newcastle, Australia, in 1976.

He has been Chair Professor in Power Engineering at Queensland University of Technology, Brisbane, Australia, since 2006. Previously, he was the Chair in Electrical Asset Management from 1998 to 2005 at the same university. He was Head of Electrical Engineering at the University of Newcastle from 1997 to 1998. Previously, he was associated with the University of Queensland from 1976 to 1994. His interests are in the areas of power systems, power electronics, and controls.

Dr. Ledwich is a fellow of I.E.Aust.

Firuz Zare (M'97–SM'06) was born in Iran in 1967. He received the Ph.D. degree in electrical engineering from Queensland University of Technology (QUT), Brisbane, Australia.

He has worked as a Development Engineer and a Consultant in industry for several years. He joined the School of Engineering Systems at QUT in 2006. His research interests are power electronic applications, pulse-width modulation techniques, renewable energy systems, and electromagnetic interferences.

Power Management and Power Flow Control With Back-to-Back Converters in a Utility Connected Microgrid

Ritwik Majumder, *Student Member, IEEE*, Arindam Ghosh, *Fellow, IEEE*, Gerard Ledwich, *Senior Member, IEEE*, and Firuz Zare, *Senior Member, IEEE*

***Abstract*—This paper proposes a method for power flow control between utility and microgrid through back-to-back converters, which facilitates desired real and reactive power flow between utility and microgrid. In the proposed control strategy, the system can run in two different modes depending on the power requirement in the microgrid. In mode-1, specified amount of real and reactive power are shared between the utility and the microgrid through the back-to-back converters. Mode-2 is invoked when the power that can be supplied by the distributed generators (DGs) in the microgrid reaches its maximum limit. In such a case, the rest of the power demand of the microgrid has to be supplied by the utility. An arrangement between DGs in the microgrid is proposed to achieve load sharing in both grid connected and islanded modes. The back-to-back converters also provide total frequency isolation between the utility and the microgrid. It is shown that the voltage or frequency fluctuation in the utility side has no impact on voltage or power in microgrid side. Proper relay-breaker operation coordination is proposed during fault along with the blocking of the back-to-back converters for seamless resynchronization. Both impedance and motor type loads are considered to verify the system stability. The impact of dc side voltage fluctuation of the DGs and DG tripping on power sharing is also investigated. The efficacy of the proposed control arrangement has been validated through simulation for various operating conditions. The model of the microgrid power system is simulated in PSCAD.**

***Index Terms*—Active and reactive power sharing, back-to-back converters, microgrid.**

I. Introduction

THE interconnection of distributed generators (DGs) to the utility grid through power electronic converters has raised concern about proper load sharing between different DGs and the grid. Microgrid can generally be viewed as a cluster of distributed generators connected to the main utility grid, usually through voltage-source-converter (VSC) based interfaces. Concerning the interfacing of a microgrid to the utility system, it is important to achieve a proper load sharing by the DGs. A load sharing with minimal communication is the best in the distribution level as the network is complex, can be reconfigured and span over a large area. The most common method is the use of droop characteristics. Parallel converters have been controlled to deliver desired real and reactive power to the system. The use of local signals as feedback to control the converters is desirable, since in a real system, the distance between the converters may make an inter-communication impractical. With this in mind, this paper proposes a configuration that is suitable for supplying electrical power of high quality to the microgrid, specifically when it is being supplied through controlled converters.

The real and reactive power sharing can be achieved by controlling two independent quantities—the frequency and the fundamental voltage magnitude [1]–[5]. The system stability during load sharing has been explored in [2] and [3]. Transient stability of power system with high penetration level of power electronics interfaced (converter connected) distributed generation is explored in [5]. While [6]–[8] explore the microgrid testing and control, [9] proposes a single-phase high-frequency ac (HFAC) microgrid as a solution towards integrating renewable energy sources in a distributed generation system. For a better performance of the DGs and more efficient power management system, it is important to achieve a control over the power flow between the grid and the microgrid. With a bidirectional control on the power flow, it is possible not only to specify exact amount of power supplied by the utility but also the fed back power from microgrid to utility during lesser power demand in the microgrid.

With number of DGs and loads connected over a wide span of the microgrid, isolation between the grid and the microgrid will always ensure a safe operation. Any voltage or frequency fluctuation in the utility side has direct impact on the load voltage and power oscillation in the microgrid side. For a safe operation of any sensitive load, it is not desirable to have any sudden change in the system voltage and frequency. The isolation between the grid and microgrid not only ensures safe operation of the microgrid load, it also prevents direct impact of microgrid load change or change in DG output voltage on the utility side.

Protection of the devices both in utility and microgrid sides during any fault is always a major concern [10]–[13]. Proper protection schemes in the distributed generation system ensure a reliable operation. Of the many schemes that have been proposed, [10] explores the effect of high DG penetration on protective device coordination and suggests an adaptive protection scheme as a solution to the problems. In [11], a method has been proposed for determining the coordination of the rate of change of frequency (ROCOF) and under/over-frequency relays for dis-

Manuscript received January 23, 2008; revised December 17, 2008. This work was supported by the Australian Research Council (ARC) through the ARC Discovery Grant DP 0774092. Paper no. TPWRS-00065-2008.

The authors are with the School of Engineering Systems, Queensland University of Technology, Brisbane, Qld 4001, Australia (e-mail: ritwik.majumder@student.qut.edu.au; a.ghosh@qut.edu.au; g.ledwich@qut.edu.au; f.zare@qut.edu.au).

Digital Object Identifier 10.1109/TPWRS.2009.2034666

tributed generation protection considering islanding detection and frequency-tripping requirements. The method is based on the concept of application region, which defines a region in the trigger time versus active power imbalance space where frequency-based relays can be adjusted to satisfy the anti-islanding and frequency-tripping requirements simultaneously.

In general, a microgrid is interfaced to the main power system by a fast semiconductor switch called the static switch (SS). It is essential to protect a microgrid in both the grid-connected and the islanded modes of operation against all faults. Inverter fault currents are limited by the ratings of the silicon devices to around 2 per unit rated current. Fault currents in islanded inverter based microgrids may not have adequate magnitudes to use traditional overcurrent protection techniques [12]. To overcome this problem, a reliable and fast fault detection method is proposed in [13].

The aim of this paper is to set up a power electronics interfaced microgrid containing distributed generators. A scheme for controlling parallel connected DGs for proper load sharing is proposed. The microgrid is connected to the utility with back-to-back converters. Bidirectional power flow control between the utility and microgrid is achieved by controlling both the converters. The back-to-back converters provide the much needed frequency and power quality isolation between the utility and the microgrid. A proper relay breaker co-ordination is proposed for protection during faults. The scheme not only ensures a quick and safe islanding at inception of the fault, but also a seamless resynchronization once the fault is cleared. The application of back-to-back converters in distributed generation would facilitate:

- controlled power flow between the microgrid and utility which can be used in case of any contractual arrangement;
- reliable power quality due to the isolation of the microgrid system from utility.

II. System Structure and Operation

A simple power system model with back to back converters, one microgrid load and two DG sources is shown in Fig. 1. A more complex case is considered in Section VIII. In Fig. 1, the real and reactive power drawn/supplied are denoted by P and Q, respectively. The back to back converters are connected to the microgrid at the point of common coupling (PCC) and to the utility grid at point A as shown in Fig. 1. Both the converters (VSC-1 and VSC-2) are supplied by a common dc bus capacitor with voltage of V_C. The converters can be blocked with their corresponding signal input BLK_1 and BLK_2. DG-1 and DG-2 are connected through voltage source converters to the microgrid. The output inductances of the DGs are indicated by inductance L_1 and L_2, respectively. The real and reactive powers supplied by the DGs are denoted by P_1, Q_1 and P_2, Q_2. While the real and reactive power demand from the load is denoted by P_L, Q_L. It is assumed that the microgrid is in distribution level with mostly resistive lines, whose resistances are denoted by R_{D1} and R_{D2}.

The utility supply is denoted by v_s and the feeder resistance and inductance are denoted, respectively, by R_s and L_s. The utility supplies P_G and Q_G to the back-to-back converters and the balance amounts $P_s - P_G$ and $Q_s - Q_G$ are supplied to

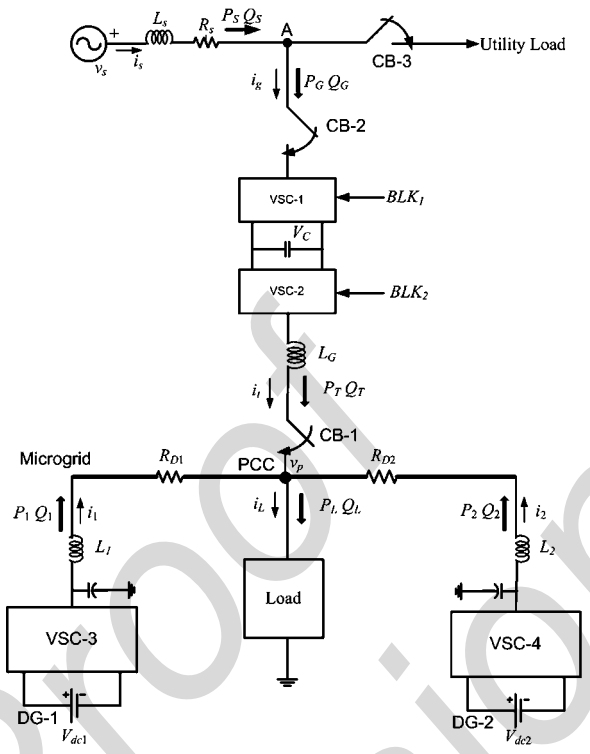

Fig. 1. Microgrid and utility system under consideration.

the utility load. The breakers CB-1 and CB-2 can isolate the microgrid from the utility supply. The power supplied from the utility side to microgrid at PCC is denoted by P_T, Q_T, where the differences $P_G - P_T$ and $Q_G - Q_T$ represent the loss and reactive power requirement of the back-to-back converter and their dc side capacitor.

The system can run in two different modes depending on the power requirement in the microgrid. In mode-1, a specified amount of real and reactive power can be supplied from the utility to the microgrid through the back-to-back converters. Rest of the load demand is supplied by the DGs. The power requirements are shared proportionally among the DGs based on their ratings. When the total power generation by the DGs is more than the load requirement, the excess power is fed back to the utility. This mode provides a smooth operation in a contractual arrangement, where the amount of power consumed from or delivered to the utility is pre-specified.

When the power requirement in the microgrid is more than the combined maximum available generation capacity of the DGs (e.g., when cloud reduces generation from PV), a pre-specified power flow from the utility to the microgrid may not be viable. The utility will then supply the remaining power requirement in the microgrid under mode-2 control, while the DGs are operated at maximum power mode. Once all the DGs reach their available power limits, the operation of the microgrid is changed from mode-1 to mode-2. While mode-1 provides a safe contractual agreement with the utility, mode-2 provides more reliable power supply and can handle large load and generation uncertainty. The rating requirement of the back to back converters will depend on the maximum power flowing through them. The maximum power flow will occur when

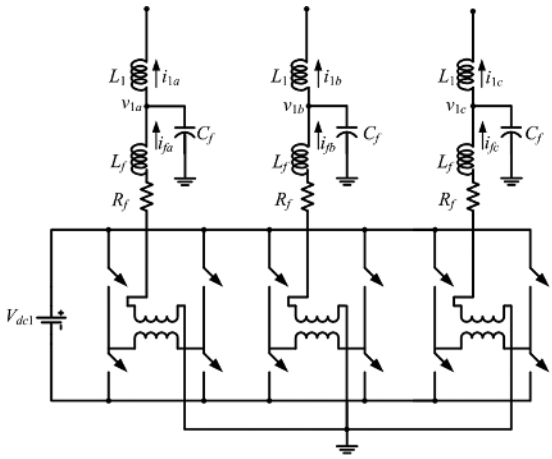

Fig. 2. Converter structure.

- the load demand in the microgrid is maximum and minimum power is generated by the DGs (power flow from utility to microgrid);
- maximum power is generated by DGs, while the load demand in the microgrid is minimum (power flow from microgrid to utility).

The rating issue has to be determined *a priori*. The microgrid cannot supply/absorb more power than the pre-specified maximum limit.

III. Converter Structure and Control

The converter structure for VSC-3 is shown in Fig. 2. DG-1 is assumed to be an ideal dc voltage source supplying a voltage of V_{dc1} to the VSC. The converter contains three H-bridges. The outputs of the H-bridges are connected to three single-phase transformers that are connected in wye for required isolation and voltage boosting [14]. The resistance R_f represents the switching and transformer losses. In this paper, an LCL filter structure is chosen to suppress the switching harmonics. This filter constitute of the leakage reactance of the transformers (L_f), the filter capacitor C_f is connected to the output of the transformers and L_1. Please note that L_1 also represents the output inductance of the DG source. The converter structure of DG-2 (VSC-4) is same as DG-1. The converters of the back-to-back converters have same structure but they are supplied by the common capacitor voltage V_C as shown in Fig. 1. It is to be noted that, while VSC-2 has an output inductance L_G (shown in Fig. 1), VSC-1 is directly connected to the point A without an output inductance. This implies that the voltage across the filter-capacitor (C_f in Fig. 2) of VSC-1 is the voltage of point A on the utility side. It is to be noted that the PSCAD simulations reported in this paper, all the converter are modeled in detail and no average linear model have been used.

All the converters are controlled in a similar way. The equivalent circuit of one phase of the converter is shown in Fig. 3. In this, $u \cdot V_{dc1}$ represents the converter output voltage, where u is the switching function that can take on values ± 1. The main aim of the converter control is to generate u.

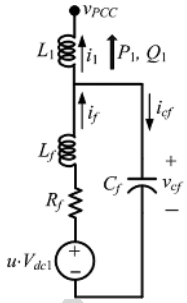

Fig. 3. Equivalent circuit of one phase of the converter.

From the circuit of Fig. 3, the state space description of the system can be given as

$$\dot{x} = Ax + B_1 u_c + B_2 v_{PCC} \tag{1}$$

where u_c is the continuous time control input, based on which the switching function u is determined. The discrete-time equivalent of (2) is

$$x(k+1) = Fx(k) + G_1 u_c(k) + G_2 v_{PCC}(k). \tag{2}$$

Let the output of the system given in (2) be v_{cf}. The reference for this voltage is given in terms of the magnitude of the rms voltage V_1^* and its angle δ_1^*. From these quantities, the instantaneous voltage references v_1^* for the three phases are generated. Neglecting the PCC voltage v_{PCC} assuming it to be a disturbance input, the input-output relationship of the system in (2) can be written as

$$\frac{v_{cf}(z)}{u_c(z)} = \frac{M(z^{-1})}{N(z^{-1})}. \tag{3}$$

The control is computed from

$$u_c(\mathrm{z}) = \frac{S(z^{-1})}{R(z^{-1})} \left\{ v_1^*(z) - v_{cf}(z) \right\}. \tag{4}$$

Then the closed-loop transfer function of the system is given by

$$\frac{v_{cf}(z)}{v_1^*(z)} = \frac{M(z^{-1})S(z^{-1})}{N(z^{-1})R(z^{-1}) + M(z^{-1})S(z^{-1})}. \tag{5}$$

The coefficients of the polynomials S and R can be chosen based on a pole placement strategy [15]. Once u_c is computed from (4), the switching function u can be generated as

$$\begin{aligned} &\text{If } u_c > h, \text{ then } u = +1 \\ &\text{elseif } u_c < -h, \text{ then } u = -1 \end{aligned} \tag{6}$$

where h is a small number.

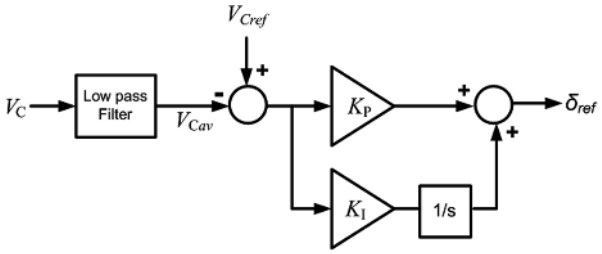

Fig. 4. Angle controller for VSC-1.

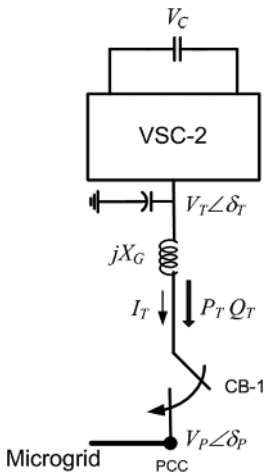

Fig. 5. Schematic diagram of VSC-2 connection to microgrid.

All the four VSCs are controlled using the above control strategy. Hence, all these controllers require their instantaneous reference voltages. These are discussed in the next two sections.

IV. Back-to-Back Converter Reference Generation

This section describe the reference generation for the back-to-back VSCs. Both the VSCs are supplied from a common capacitor of voltage V_C as shown in Fig. 1. Depending on the power requirement in the microgrid, there are two modes of operation as discussed in Section II. However the reference generation for VSC-1 is common for both these modes. This is discussed next.

A. VSC-1 Reference Generation

Reference angle for VSC-1 is generated as shown in Fig. 4. First the measured capacitor voltage V_C is passed through a low pass filter to obtain V_{Cav}. This is then compared with the reference capacitor voltage V_{Cref}. The error is fed to a PI controller to generate the reference angle δ_{ref}. VSC-1 reference voltage magnitude is kept constant, while angle is the output of the PI controller. The instantaneous voltages of the three phases are derived from them.

The two modes of VSC-2 reference generation are discussed next.

B. VSC-2 Reference Generation in Mode-1

VSC-2, which is connected with PCC through an output inductance L_G, controls the real and reactive power flow between the utility and the microgrid. Fig. 5 shows the schematic diagram of this part of the circuit, where the voltages and current are shown by their phasor values.

Let us assume that, in mode-1 the references for the real and reactive power be P_{Tref} and Q_{Tref}, respectively, and the VSC-2 output voltage be denoted by $V_T\angle\delta_T$ and the PCC voltage by $V_P\angle\delta_P$. Then the reference VSC-2 voltage magnitude and its can be calculated as

$$V_T = \frac{V_P^2 + Q_{Tref}X_G}{V_P\cos(\delta_T - \delta_P)} \tag{7}$$

$$\delta_T = \tan^{-1}\left(\frac{P_{Tref}X_G}{V_P^2 + Q_{Tref}X_G}\right) + \delta_P. \tag{8}$$

Depending on the real and reactive power demand, these references are calculated, based on which the instantaneous reference VSC-2 voltages for the three phases are computed. It is to be noted that, sign of the active and reactive power references are taken as negative when it is desired to supply the power from the microgrid to the utility side.

C. VSC-2 Reference Generation in Mode-2

In mode-2, the utility supplies any deficit in the power requirement through back-to-back converters while the DGs supply their maximum available power. Let the maximum rating of the back-to-back converters be given by P_{Tmax} and Q_{Tmax}. Then the voltage magnitude and angle reference of VSC-2 is generated as

$$\begin{aligned}\delta_T &= \delta_{T\max} - m_T \times (P_T - P_{T\max}) \\ V_T &= V_{T\max} - n_T \times (Q_T - Q_{T\max})\end{aligned} \tag{9}$$

where V_{Tmax} and δ_{Tmax} are the voltage magnitude and angle, respectively, when it is supplying the maximum load. The VSC-2 droop coefficient m_T and n_T are chosen such that the voltage regulation is within acceptable limit from maximum to minimum power supply.

V. Reference Generation for DG Sources

In this section, the reference generation for the DGs is presented. It is to be noted that the reference generations of the DGs are different from reference generation of the back-to-back converters. The control strategy for both the DGs is the same and hence only DG-1 reference generation is discussed here.

A. Mode-1

It is assumed that in mode-1 the utility supplies a part of the load demand through the back-to-back converters and rest of the power demand in the microgrid is supplied and regulated by the DGs. The output voltages of the converters are controlled to share this load proportional to the rating of the DGs. As the output impedance of the DG sources is inductive, the real and reactive power injection from the source to microgrid can be controlled by changing voltage magnitude and its angle. Fig. 6 shows the power flow from DG-1 to microgrid where the

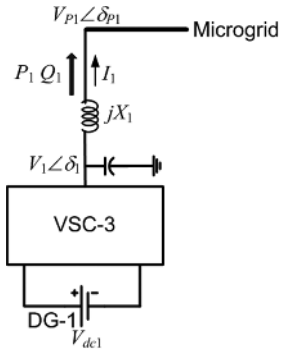

Fig. 6. Power flow from DG-1 to microgrid.

voltages and current are shown in rms values and the output impedance is denoted by jX_1.

The real and reactive power flow from DG to microgrid can be calculated as

$$P_1 = \frac{V_1 \times V_{P1}\sin(\delta_1 - \delta_{P1})}{X_1}$$
$$Q_1 = \frac{V_1^2 - V_1 \times V_{P1}\cos(\delta_1 - \delta_{P1})}{X_1}. \quad (10)$$

It is to be note that VSC-3 does not have any direct control over $V_{P1}\angle\delta_{P1}$. The output inductances of the DGs decouple the real and reactive power at the DG output. Hence from (10), it is clear that if the angle difference $(\delta_1 - \delta_{P1})$ is small, the real power can be controlled by controlling δ_1, while the reactive power can be controlled by controlling V_1. Thus the power requirement can be distributed among the DGs, similar to a conventional droop by dropping the voltage magnitude and angle as

$$\delta_1 = \delta_{1rated} - m_1 \times (P_1 - P_{1rated})$$
$$V_1 = V_{1rated} - n_1 \times (Q_1 - Q_{1rated}) \quad (11)$$

where V_{1rated} and δ_{1rated} are the rated voltage magnitude and angle, respectively, of DG-1, when it is supplying the load to its rated power levels of P_{1rated} and Q_{1rated}. The coefficients m_1 and n_1 respectively indicate the voltage angle drop vis-à-vis the real power output and the magnitude drop vis-à-vis the reactive power output. These values are chosen to meet the voltage regulation requirement in the microgrid. It is assumed that all the DGs are all converter based and so the output voltage angle can be changed instantaneously. The angle droop will be able to share the load without any drop in system frequency. In a microgrid with frequency droop, the variation of with normal load changes tends to be much higher than system grid frequency variation. In trying to correct this using low droop coefficient may lead to large variations in the frequency. Angle droop avoids this variation in frequency to some extent. A comparison of performance between angle and frequency droop is discussed in Appendix A.

To show the power sharing with angle droop, two DGs with a load is considered as shown in Fig. 7. The voltages and the

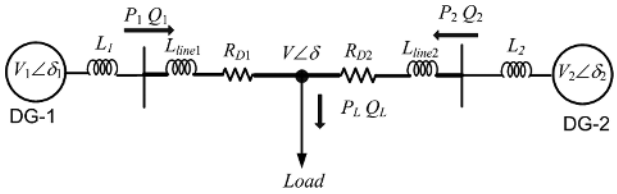

Fig. 7. Power sharing among the DGs.

power flow are indicated in the figure. Applying dc load flow with all the necessary assumptions, we get

$$\delta_1 - \delta = (X_1 + X_{L1})P_1$$
$$\delta_2 - \delta = (X_2 + X_{L2})P_2 \quad (12)$$

where $X_1 = \omega L_1/(V_1V)$, $X_2 = \omega L_2/(V_2V)$, $X_{L2} = \omega L_{Line2}/(V_2V)$, and $X_{L1} = \omega L_{Line1}/(V_1V)$. The angle droop equation of the DGs is given by

$$\delta_1 = \delta_{1rated} - m_1 \times (P_1 - P_{1rated})$$
$$\delta_2 = \delta_{2rated} - m_2 \times (P_2 - P_{2rated}). \quad (13)$$

The offset in the angle droop is taken such that when DG output power is zero, the DG source angle is zero. For this the rated droop angles are taken as $\delta_{1rated} = m_1P_{1rated}$ and $\delta_{2rated} = m_2P_{2rated}$. Then from (13), we get

$$\delta_1 - \delta_2 = -m_1P_1 + m_2P_2. \quad (14)$$

Similarly from (12), we get

$$\delta_1 - \delta_2 = (X_1 + X_{L1})P_1 - (X_2 + X_{L2})P_2. \quad (15)$$

Assuming the system to be lossless, we can find from Fig. 7 that $P_2 = P_L - P_1$ and substituting this (14) and (15), we get

$$(X_1 + X_{L1})P_1 - (X_2 + X_{L2})(P_L - P_1)$$
$$= -m_1P_1 + m_2(P_L - P_1)$$
$$\Rightarrow P_1 = \frac{X_2 + X_{L2} + m_2}{X_2 + X_{L2} + m_2 + X_1 + X_{L1} + m_1}P_L. \quad (16)$$

Similarly P_2 can be calculated as

$$P_2 = \frac{X_1 + X_{L1} + m_1}{X_2 + X_{L2} + m_2 + X_1 + X_{L1} + m_1}P_L. \quad (17)$$

From (16) and (17), the ratio of the output power is calculated as

$$\frac{P_1}{P_2} = \frac{X_2 + X_{L2} + m_2}{X_1 + X_{L1} + m_1}. \quad (18)$$

It is to be noted that the value of X_1 and X_2 are very small compared to the value of m_1 and m_2 (m_1 is ten times of X_1 in the example where $X_1 = 0.02595$ rad/MW). Moreover since the microgrid line is considered to be mainly resistive with low line inductance and the DG output inductance is much larger, we can write

$$m_1 \gg X_1 \gg X_{L1} \text{ and } m_2 \gg X_2 \gg X_{L2}.$$

Therefore, from (18), it is evident that the droop coefficients play the dominant role in the power sharing. As the droop coefficients are taken as inversely proportional to the DG rating, from (18), we can write

$$\frac{P_1}{P_2} \approx \frac{m_2}{m_1} = \frac{P_{1rated}}{P_{2rated}}. \tag{19}$$

The error is further reduced by taking the output inductance (L_1, L_2) of the DGs inversely proportional to power rating of the DGs. If the microgrid line is inductive in nature, and of high value, then network knowledge is needed to minimize the error by choosing the DG output inductance such that

$$\frac{X_1 + X_{line1}}{X_2 + X_{line2}} = \frac{P_{2rated}}{P_{1rated}}.$$

The system shown in Fig. 7 is a very simple example to show the power sharing. In a real system with number of DGs and loads in different locations, line impedances will have an impact on the load sharing. But for a microgrid within a small geographical area, the line inductances will never be very high. Moreover a high droop coefficient will always play a dominant role and share the power as desired with a very small deviation. The reactive power has been shared with the conventional voltage magnitude drop [1]–[4]. Since the converter output impedance is inductive, the change in output voltage angle does not have a significant effect on the reactive power sharing.

Thus DG-1 can supply the desired power if the output voltage of VSC-3 has magnitude and angle as given in (11). From the rms quantities the instantaneous reference voltages of the three phases are obtained. In a similar way, the instantaneous reference voltages for VSC-4 are also obtained. This method of load sharing is based only on local measurements and does not need intercommunication between the DGs. For the determination of the phase angles, a common reference is used. This can easily accomplished through a Global Positioning System (GPS) synchronizing signal. It is to be noted that the conventional frequency droop method can realize the real power sharing without such a GPS signal.

B. Mode-2

In mode-2, the DGs supply their maximum available power. The reference generation for the DGs in mode-2 is similar to the reference generation of VSC-2 of back-to-back converter in mode-1 as given in (7) and (8). Let us denote the available active power as P_{1avail}. Then based on this and the current rating of the DG, the reactive power availability Q_{1avail} of the DG can be determined. Based on these quantities, the voltage references as shown in Fig. 6 are calculated as

$$V_1 = \frac{V_{P1}^2 + Q_{1avail}X_1}{V_{P1}\cos(\delta_{P1} - \delta_P)} \tag{20}$$

$$\delta_1 = \tan^{-1}\left(\frac{P_{1avail}X_1}{V_{P1}^2 + Q_{1avail}X_1}\right) + \delta_{P1}. \tag{21}$$

The references for the other DGs are generated in a similar way.

VI. Relay and Circuit Breaker Coordination During Islanding and Resynchronization

The reference generations described in Section IV for DGs and back-to-back converters are totally independent of each other. In mode-1, once the desired value of real and reactive power flow through the back-to-back converters is set, the rest of the required power will automatically be shared amongst the DGs. In mode-2, the DGs supply their maximum available power while the extra the power requirement from utility is supplied through the back-to-back converter. When a DG reaches its maximum available power, it broadcasts it to VSC-2 control center. The mode change is initiated when all the DGs reach their available limits. Note that other than the broadcast signals, no other communication is needed between the back-to-back converters and the DGs, even during islanding and resynchronization. But proper relay breaker coordination, along with converter blocking, will be required to maintain the voltage of the dc capacitor during islanding and resynchronization. Fig. 8 shows the logic diagram used for this purpose, where *Trip_Signal* initiates the tripping of CB-2 (Fig. 1) and the signal BLK_1 blocks VSC-1. The same logic is also used for the tripping CB-1 and the blocking of VSC-2. The rate of rise of current i_g is monitored by the protection scheme. When it exceeds a threshold value in response to a fault in the utility grid, the output of the *Protection Scheme* (Fig. 8) becomes high. This output is used to set all the RS flip flops. The upper flip flop (F/F-1) generates the trip signal. This flip flop is reset by the *Fault_Clear* signal. The lower two flip flops, F/F-2 and F/F-3 generate BLK_1 and BLK_2 signals, respectively. The blocking deactivation is initiated when the fault is cleared and *Fault_Clear* signal is set high manually. The converter VSC-1 is deblocked by resetting F/F-2 when the breaker CB-2 is closed, as indicated by *Br_Status* signal. The AND gate insures that no false deblocking occurs till both these signals are high. VSC-2 is deblocked after VSC-1 is deblocked. This is why *Fault_Clear* signal is passed through a time delay circuit to generate the reset signal for F/F-3.

Fig. 9 shows the timing diagram of the breakers and converter blocking during islanding and resynchronization process. If a breaker is closed, the signal *Br_Status* is high and it goes low when the breaker opens. As evident from Fig. 8, the output of the *Protection Scheme* triggers the RS flip flops, which simultaneously generates both the trip and block signals. The block signals blocks both VSC-1 and VSC-2 simultaneously. Once the trip signals goes high, the breakers CB-1 and CB-2 open after a finite time delay (t_op) as indicated in Fig. 9. Unless the two VSCs are blocked, the dc capacitor voltage collapses due to the sudden increase in power requirement on the utility side. Also

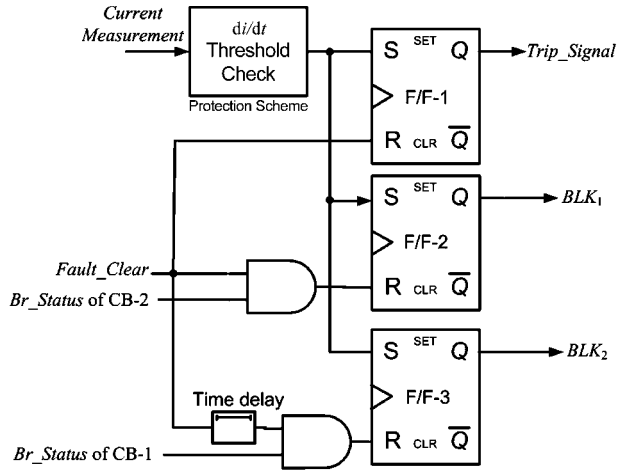

Fig. 8. Logic for breaker operation and converter blocking.

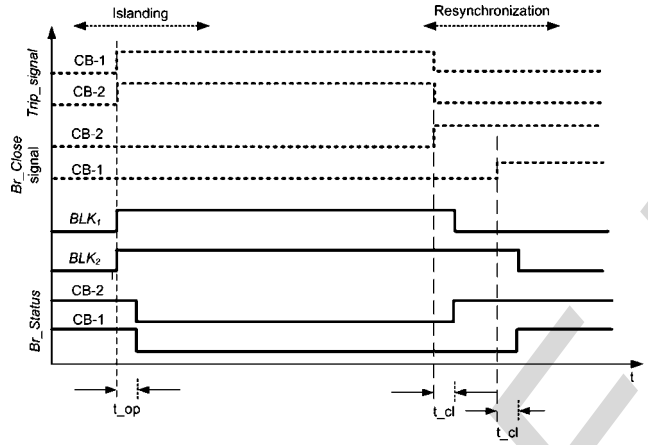

Fig. 9. Breakers and converter blocking timing diagram.

to prevent the angle reference δ_{ref} from diverging during the contingency, the angle controller of Fig. 4 is bypassed and the reference is held at the pre-fault value. Note that, once a breaker opens, the *Protection Scheme* output goes low causing the set input of the flip flops of Fig. 8 to become 0.

During islanding, breakers CB-1 and CB-2 are opened simultaneously. However during resynchronization, CB-2 is closed and VSC-1 is deblocked first connecting this to the utility. This will cause the dc capacitor voltage to rise taking a finite time depending on the capacitor voltage drop during islanding. Once the capacitor voltage settles to its reference value and the angle controller of Fig. 4 settles, CB-1 is closed and VSC-2 is deblocked.

Once the fault is cleared, *Fault_Clear* signal is set high manually. This signal is the same as *Br_Close* signal of CB-2. The *Fault_Clear* signal also resets *Trip_signal*, used both by CB-1 and CB-2. With a finite time delay (t_cl) from the initiation of *Br_Close* signal, CB-2 closes, making the *Br_Status* signal for CB-2 high. This resets F/F-2 and deactivates BLK_1 signal causing switching devices of VSC-1 to start conducting. As mentioned earlier and shown in Fig. 8, *Br_Close* signal for CB-1 is generated after a time delay from the *Fault_Clear* signal. Once this signal is generated, CB-1 closes after a time delay t_cl. This then resets F/F-3 and VSC-2 starts conducting. To even further safeguard the dc capacitor voltage, the power flow reference for VSC-2 is switched to zero during islanding and brought back to its previous value after resynchronization. This step by step process ensures a seamless resynchronization.

TABLE I
SYSTEM AND CONTROLLER PARAMETERS

System Quantities	Values
Systems frequency	50 Hz
Source voltage (V_s)	11 kV rms (L-L)
Feeder impedance	R_s = 3.025 Ω, L_s = 57.75 mH
Load	
Impedance (Balanced)	R_L = 100.0 Ω, L_L = 300.0 mH
or	
Induction motor	Rated 40 hp, 11 kV rms (L-L)
DGs and VSCs	
DC voltage (V_{dc1}, V_{dc2})	3.5 kV
Transformer rating	3 kV/11 kV, 0.5 MVA, 2.5% reactance (L_f)
VSC losses (R_f)	1.5 Ω
Filter capacitance (C_f)	50 μF
Inductances (L_1, L_2)	20 mH and 16.0 mH
Inductances (L_G)	28.86 mH
Hysteresis constant (h)	10^{-5}
Angle Controller	
Proportional gain (K_P)	– 0.2
Integral gain (K_I)	– 5.0
Droop Coefficients	
Power–angle	
m_1	0.3 rad/MW
m_2	0.24 rad/MW
Voltage–Q	
n_1	0.15 kV/MVAr
n_2	0.12 Kv/MVAr

VII. SIMULATION STUDIES

Simulation studies are carried out in PSCAD/EMTDC (version 4.2). Different configurations of load and its sharing are considered. The DGs are considered as inertia-less dc source supplied through a VSC. The system data are given in Table I. The droop coefficients are chosen such that both active and reactive powers of the load are divided in a ratio of 1:1.25 between DG-1 and DG-2. Some of the simulation results to indicate the accuracy of the proposed control are listed in Table II, given in Appendix B.

A. Case-1: Load Sharing of the DGs With Utility

If the power requirement of the load in microgrid is more than the power generated by the DGs, the balance power is supplied by the utility through the back-to-back converters. The desired power flow the utility to the microgrid is controlled by (7) and (8), while droop (10) controls the sharing of the remaining power. It is desired that 50% of the load is supplied by the utility and rest of the load is shared by DG-1 and DG-2. The impedance load of Table I is considered for this case. Fig. 10 shows the real and reactive power sharing between utility and the DGs. Fig. 11(a) shows the phase-a reference and output voltage, whereas three-phase voltage tracking error is shown in Fig. 11(b). It can be seen that the tracking error is less than 0.2%. Fig. 12 shows the capacitor voltage and the output of the angle controller. At 0.1 s, the impedance of the load is halved and at 0.35 s, it is changed back to its nominal value. It can be seen

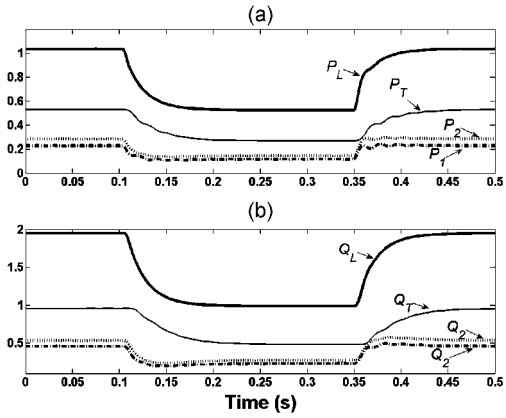

Fig. 10. Real and reactive power sharing for Case-1. (a) Real power sharing (MW). (b) Reactive power sharing (MVAr).

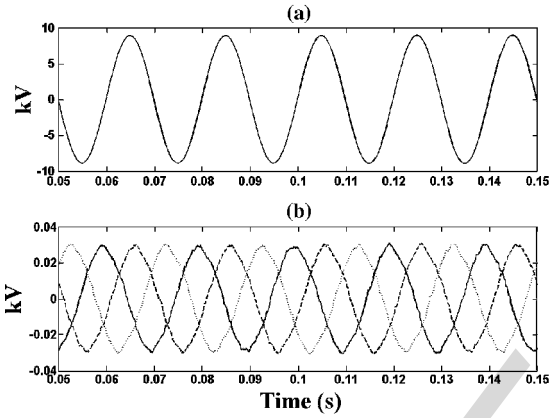

Fig. 11. Voltage tracking of DG-1 Case-1. (a) Phase-a references and output voltages of DG-1. (b) Voltage tracking errors of the three phases of DG-1.

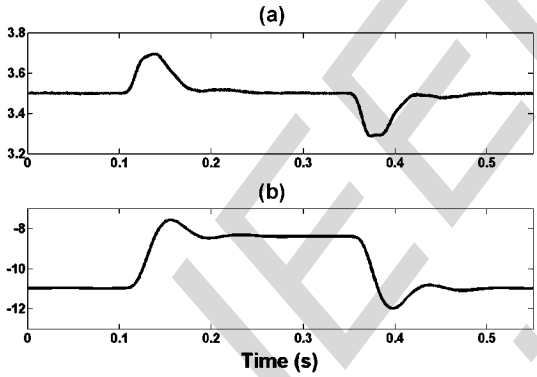

Fig. 12. Capacitor voltage and angle controller output for Case-1. (a) Capacitor voltage (kV). (b) Angle controller output (degree).

that the system goes through minimal transient and reaches its steady state within five cycles (100 ms) for both the transients.

B. Case-2: Change in Power Supply From Utility

If the power flow from the utility to the microgrid is changed by changing the power flow references for VSC-2, the extra power requirement is automatically picked up by the DGs. Fig. 13 shows the real and reactive power sharing, where at 0.1 s the power flow from the utility is changed to 20% of the total load from the initial value of 50% as considered in

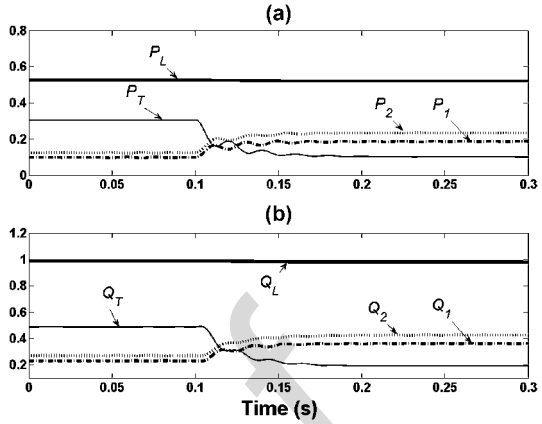

Fig. 13. Real and reactive power sharing for Case-2. (a) Real power sharing (MW). (b) Reactive power sharing (MVAr).

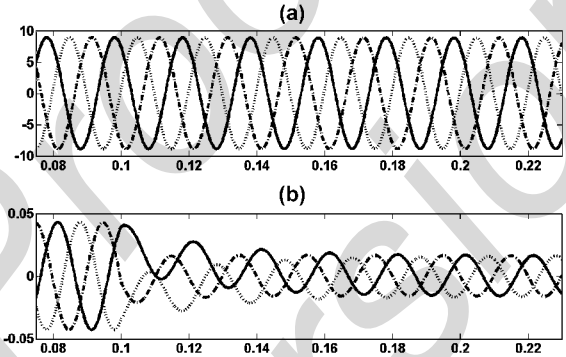

Fig. 14. Three-phase PCC voltage and injected current for Case-2. (a) Three-phase PCC voltage (kV). (b) Three-phase current injected at PCC by back-to-back inverter (kA).

Case-1. It can be seen that the DGs pick up the balance load demand and share it proportionally as desired. The unchanged real and reactive load power during the change over proves the efficacy of the controller for smooth transition. Fig. 14 shows the PCC voltage and change in current injection at PCC from utility. It can be seen that the PCC voltage remained balanced and transient-free, while the injected currents reach steady state within four cycles.

C. Case-3: Power Supply From Microgrid to Utility

When the power generation of the DGs is more than the power requirement of the load, excess power can be fed back to the utility through the back-to-back converters. It is desired that the utility supplies 50% of the microgrid load initially. At 0.1 s, however, the same amount of power is fed back to the utility by changing the sign of the power flow reference for the back-to-back converters. The DG output increases automatically to supply the total load power and power to the utility, as evident from Fig. 15.

Fig. 16(a) shows the phase-a voltage at PCC and phase-a current injected from the utility to the microgrid, where current is scaled up 30 times. The change in the power flow direction is indicated by the sudden change in phase of the injected current phase at 0.1 s, vis-à-vis that of the voltage. Fig. 16(b) shows the three-phase current injected by the utility to the microgrid. It reaches steady state within three cycles. Apart from the phase

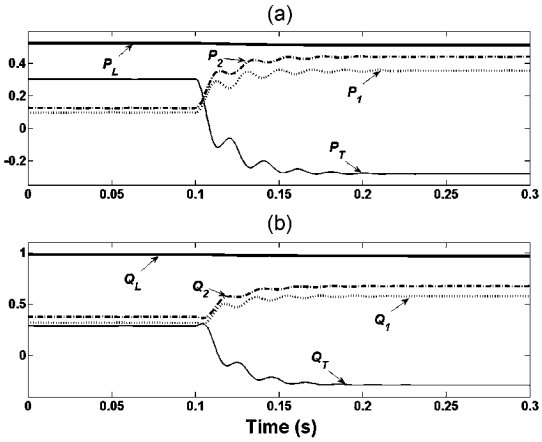

Fig. 15. Real and reactive power sharing during power reversal (Case-3). (a) Real power sharing (MW). (b) Reactive power sharing (MVAr).

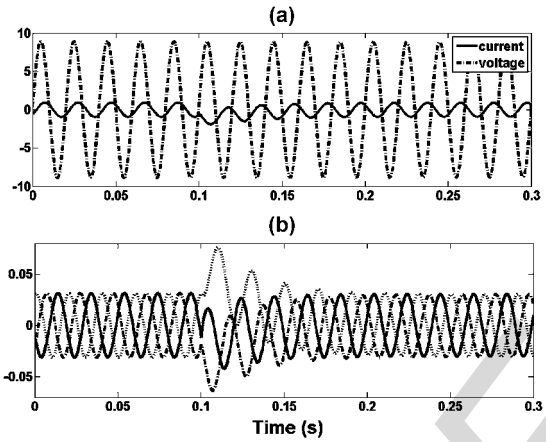

Fig. 16. PCC voltage and injected current for Case-3. (a) Phase-a PCC voltage (kV) and phase-a current from utility to microgrid (kA), scaled up 30 times. (b) Three-phase current injected from utility to microgrid (kA).

reversal, the magnitude of the currents remain the same, indicating that the same amount of power flow is taking place, albeit in the opposite direction.

D. Case-4: Load Sharing With Motor Load

In this section, load sharing with the induction motor load, given in Table I, is investigated. An impedance load is an infinite sink as it can absorb any change in the instantaneous real and reactive power. However an inertial load such as motor is not capable of that. Thus any sudden big change in the terminal voltage results in large oscillation in the real and reactive power. At the beginning it is assumed that the utility supplies 0.2 MW of real power and 0.5 MVAr of reactive power to the microgrid. Then at 0.05 s, the power reference is changed such that the utility supplies 0.3 MVAR of reactive power and no real power. The power sharing results for this case are shown in Fig. 17.

E. Case-5: Change in Utility Voltage and Frequency

One of the major advantages of the back-to-back converter connection is that it can provide isolation between the utility and the microgrid, both for voltage and frequency fluctuations.

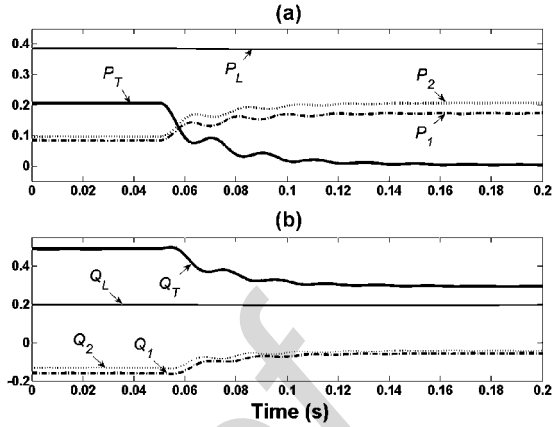

Fig. 17. Real and reactive power sharing with motor load (Case-4). (a) Real power sharing (MV). (b) Reactive power sharing (MVAr).

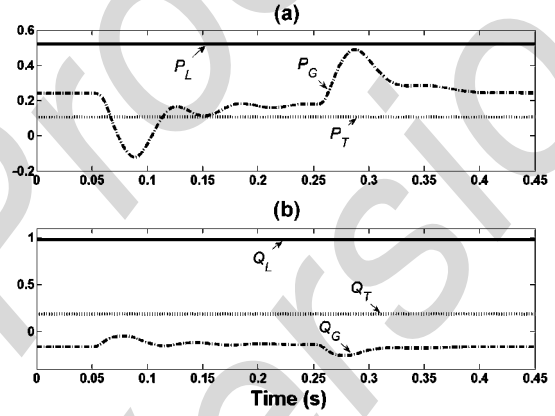

Fig. 18. Real and reactive power during frequency fluctuation (Case-5). (a) Real power (MW). (b) Reactive power (MVAr).

Fig. 18 shows the system response for frequency fluctuation in the utility side from 0.05 s to 0.25 s. At 0.05 s, the utility frequency dropped by 0.5%, and at 0.25 s, it comes back to its initial value of 50 Hz. The real and reactive power injections from utility to VSC-1 are shown as $P_{\rm G}$ and $Q_{\rm G}$, respectively. It can be seen that while $P_{\rm G}$ and $Q_{\rm G}$ fluctuate, the load power (P_L, Q_L) and the injected power to the microgrid (P_T, Q_T) remain constant.

With the system operating in steady state, a 50% balanced sag in the source voltage occurs in 0.1 s. The sag is removed after 0.5 s. Fig. 19 shows the power and the reactive power during this condition. It can be seen that the load power (P_L, Q_L) and the injected power to the microgrid (P_T, Q_T) remain almost undisturbed. The real power drawn from the grid (P_G), barring transients at the inception and removal of the sag, is maintained at the steady state level in order to supply power to the microgrid. The reactive power (Q_G) however reverses sign as the utility voltage drop causing it to absorb reactive power. During the sag, the dc capacitor supplies reactive power to the utility. The dc capacitor voltage and the output of the angle controller are shown in Fig. 20. It can be seen that while the dc capacitor voltage is maintained at its pre-specified value, the angle drops in sympathy with the source voltage drop to maintain the

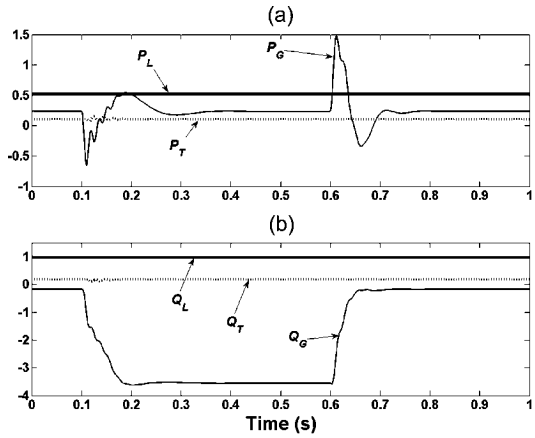

Fig. 19. Real and reactive power during voltage sag (Case-5). (a) Real power (MW) during voltage sag. (b) Reactive power (MVAr) during voltage sag.

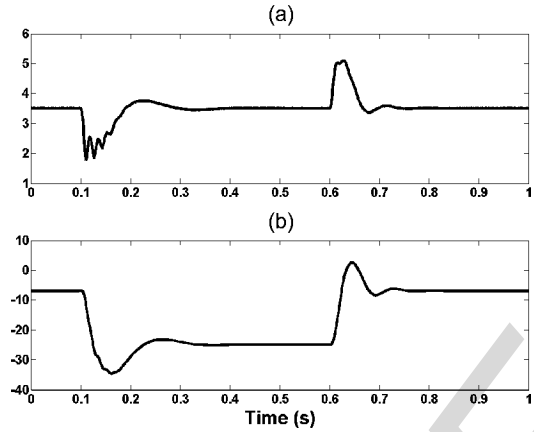

Fig. 20. DC capacitor voltage and angle controller output during voltage sag. (a) DC capacitor voltage (kV). (b) Angle controller output (degree).

injected power constant. The angle returns to its pre-sag value once the sag is removed.

F. Case-6: Islanding and Resynchronization

In this section the system response during a fault in the utility is investigated. Let us assume that a single-line to ground fault occurs at point F, which is half way between the utility source and point A, as shown in Fig. 21. As the fault occurs, the trip signal for the breakers CB-1 and CB-2 are initiated by the protection scheme which measure the rate of rise of current i_g. But breakers need a finite time to physically open the contact. During this time, the back to back converters start feeding the fault as shown by $P_{\rm G}, Q_{\rm G}$ in Fig. 21, which will result in the collapse of the capacitor voltage $V_{\rm C}$. As explained in Section VI, the coordination of breaker tripping and VSC blocking is required to avoid the voltage collapse.

With the system operating in steady state, the single-line to ground fault in phase-a occurs at 0.05 s and the fault is cleared at 0.1 s. The resynchronization process starts at 0.25 s when the *Br_Close* signal of CB-2 is generated. Subsequently, at 0.35 s, the *Br-Close* signal of CB-1 is generated. The dc capacitor voltage and the angle controller output are shown in Fig. 22 in which the angle controller output is kept constant to its pre-fault

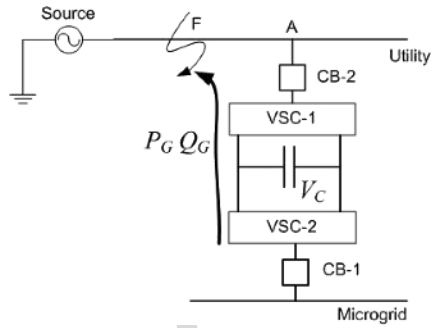

Fig. 21. Location of the single-line to ground fault.

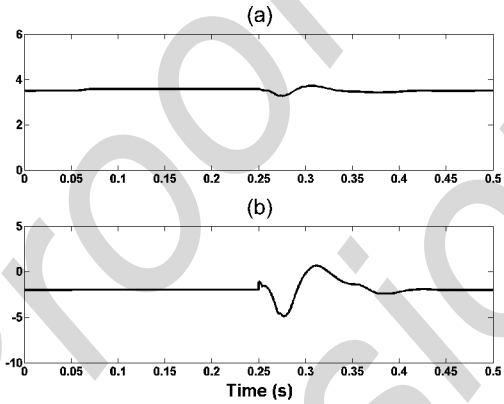

Fig. 22. DC capacitor voltage and angle controller output during islanding and resynchronization (Case-6). (a) Capacitor voltage (kV). (b) Angle controller output (degree).

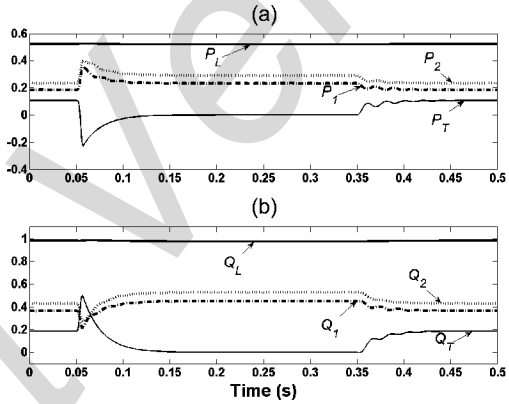

Fig. 23. Real and reactive power during islanding and resynchronization (Case-6). (a) Real power sharing (MW). (b) Reactive power sharing (MVAr).

value between 0.05 s to 0.25 s. Fig. 23 shows real and reactive power sharing, which are in accordance to the desired objective to keep microgrid load power constant.

G. Case-7: Variable Power Supply From Utility

In cases presented above, it has been assumed that the system is running in mode-1 where DGs can supply the balance of the load requirement once the pre-specified amount of power is drawn from the utility. The following example shows the switch from mode-1 to mode-2 when the maximum available power that can be supplied by the DGs is reached. Initially, the microgrid is running in mode 1. At 0.1 s, the input power from

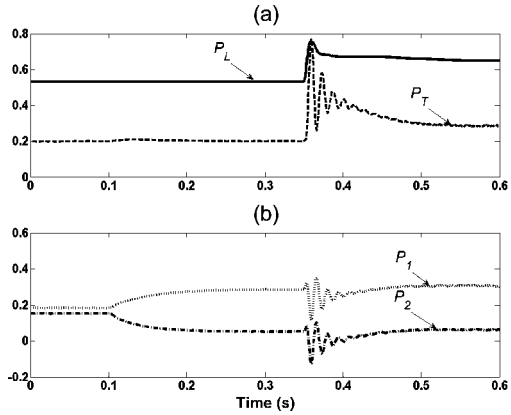

Fig. 24. Real power sharing during power limit and mode change (Case-7). (a) Real power demand from load and supply through utility (MW). (b) Real power sharing by the DGs (MW).

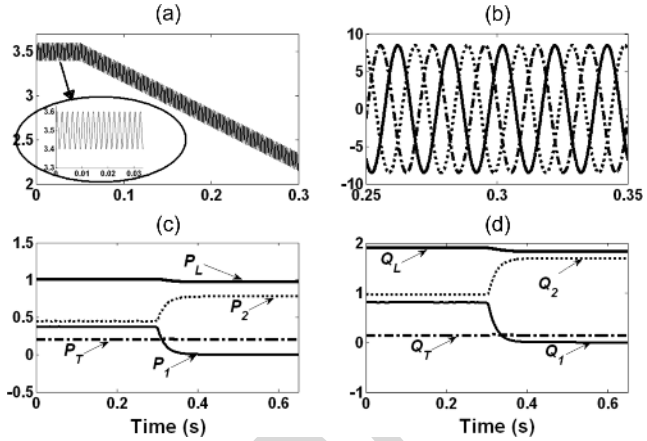

Fig. 25. DC voltage fluctuation in DG-1 and its tripping (Case-8). (a) DC voltage fluctuation (kV). (b) v_{p1} (kV). (c) Real power sharing (MW). (d) Reactive power sharing (MVAr).

DG-1 (P_{1avail}) suddenly reduces to 60 KW. DG-2 then supplies the shortfall as can be seen in Fig. 24. The load power and that supplied by the utility remain unchanged. Subsequent to this, suddenly the load changes at 0.35 s in which the power demand in the microgrid increases from 0.53 MW to 0.64 MW. However, the maximum power that can be supplied by DG-2 is set at 300 kW. This implies that both the DGs together can supply 360 KW. Moreover, the utility grid was supplying 200 kW before this event. Therefore an additional 80 KW of power is required from the utility grid and hence a mode change is inevitable. This mode change is initiated with VSC-2 droop gains of $m_T = 0.03$ rad/MW and $n_T = 0.02$ kV/MVAr. The results are also shown in Fig. 24. It can be seen that there is no appreciable overshoot in the active powers supplied by the DGs. The utility power (P_T) rises sharply in order to supply the load demand. The system settles in five cycles.

H. Case-8: DC Voltage Fluctuation and Loss of a DG

Photovoltaic (PV) cells are the most common form of converter interfaced DGs. The power output from these cells may vary during the day and may also have fluctuations depending on the atmospheric conditions. However as long as the dc voltage remains above a threshold, the converter tracks the output voltage reference. If the voltage falls below this threshold, the converter is switched off and the utility and the other DGs will have to share the microgrid load. To prove this point, a simulation is carried out in which it is assumed that DG-2 is capable of supplying the excess load demand, while the utility supplies the pre-specified amount of power in mode-1. If this is not possible, a switch to mode-2 will be necessary, which is not shown here.

The simulation results for this case are shown in Fig. 25. The dc voltage of DG-1 has a sinusoidal fluctuation of 3% and at 0.05 s, it starts ramping down as in Fig. 25(a). The 500-Hz fluctuation is shown in the inset. At 0.3 s, when the dc voltage falls below 2.25 kV, this DG is isolated from the system. Since the other DG picks up the load, any appreciable drop in v_{p1} (Fig. 6) does not occur as evident from Fig. 25(b). Fig. 25(c) and (d) shows the real and reactive powers, respectively. It can be seen that there is a slight drop in the load power indicating a slight microgrid voltage drop. However the utility power remains unchanged and that supplied by DG-2 increases.

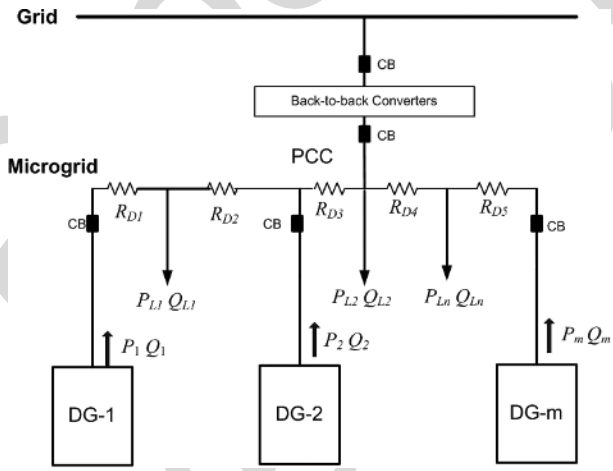

Fig. 26. Microgrid structure with large number of DGs and loads.

VIII. Microgrid Containing Multiple DGs

In the studies presented so far, it has been assumed that only two DGs and a load are connected to the microgrid. In general, however, there might be several DGs and loads connected to it, as shown in Fig. 25. It is assumed that there are a total number of n loads and m DGs. The total active and reactive powers consumed by the loads are given by

$$\begin{aligned} P_L &= P_{L1} + P_{L2} + \cdots + P_{Ln} \\ Q_L &= Q_{L1} + Q_{L2} + \cdots + Q_{Ln}. \end{aligned} \tag{22}$$

The required power will be shared by DGs depending on their rating, given by

$$\begin{aligned} m_1 \times P_{1rated} &= m_2 \times P_{2rated} = \cdots = m_m \times P_{mrated} \\ n_1 \times Q_{1rated} &= n_2 \times Q_{2rated} = \cdots = n_m \times Q_{mrated}. \end{aligned} \tag{23}$$

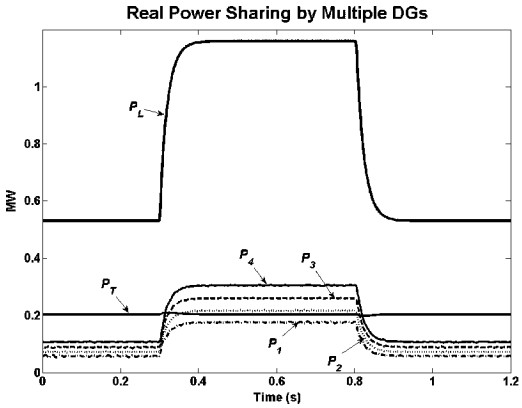

Fig. 27. Real power sharing with four DGs.

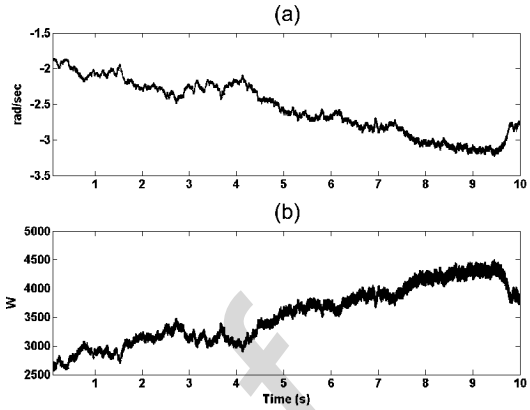

Fig. 28. Frequency deviation with frequency droop control. (a) Frequency deviation with frequency droop (DG-2). (b) Power output with frequency droop (DG-2).

However, like any droop method, the different line impedance between the load connection points, throughout the microgrid will have slight impact on the load sharing. The reference generation for the DGs will remain the same as before.

To validate a proper load sharing with multiple DGs, two more DGs are connected to the microgrid. The DG parameters, output impedance, converter structure and controller are the same as those used for DG-1 and DG-2. The droop coefficients for the four DGs are chosen such that they share both real and reactive power in the ratio of DG-1: DG-2: DG-3: DG-4 equal to 1:1.25:1.55:1.72. The load is also distributed in three different places to achieve a microgrid structure similar as shown in Fig. 26 with $m = 4$ and $n = 3$. Fig. 27 shows the real power sharing, where the load power demand is doubled at 0.3 s, and brought back to initial value at 0.8 s. It is evident from the figure that a proper load sharing occurs in the desired ratio.

IX. Conclusions

In this paper, a load sharing and power flow control technique is proposed for a utility connected microgrid. The utility distribution system is connected to the microgrid through a set of back-to-back converters. In mode-1, the real and reactive power flow between utility and microgrid can be controlled by setting the specified reference power flow for back-to-back converters module. Rest of the power requirement in the microgrid is shared by the DGs proportional to their rating. In case of high power demand in the microgrid, the DGs supply their maximum power, while rest of the power demand is supplied by utility through back-to-back converters (mode-2). A broadcast signal can be used by the DGs to indicate their mode change. However only locally measured data are used by the DGs and no communication is needed for the load sharing. The utility and microgrid are totally isolated, and hence, the voltage or frequency fluctuations in the utility side do not affect the microgrid loads. Proper switching of the breaker and other power electronics switches has been proposed during islanding and resynchronization process. The efficacy of the controller and system stability is investigated in different operating situation with various types of loads.

Appendix A

To show the relative differences between the angle and frequency droop controllers, we have chosen a simple system as shown in Fig. 7. The frequency droop controller is given by [1]–[4]

$$\omega = \omega_{ref} - m(P - P_{ref}). \tag{A1}$$

The output impedances of the two sources are chosen in a ratio of 1:1.33 and the powers are also chosen in the ratio of 1.33:1. No reactive power droop has been used and the voltage magnitudes are held constant. Both frequency and angle droop controller gains are chosen at 50% of their respective marginal stability points. The VSCs and DGs ratings for both cases are assumed to be identical.

The load in Fig. 7 is assumed to be resistive. To represent random changes of customer load, the conductance is chosen as the integral of a Gaussian white noise source with zero mean and standard deviation of 0.01 Mho. The output inductances of the two converters are 25 mH and 18.8 mH. The impedance of line 1 is $0.25 + j1.6$ while impedance of line 2 is $0.1 + j0.95$. Fig. 28 shows the steady state frequency variation and power output of DG-2 with frequency droop controller, while those with angle droop controller are shown in Fig. 29. It can be seen that with the frequency droop controller, the relation between frequency deviation and power output obeys (A1). A similar relationship also exists between angle and output power with angle droop control (11), which is not shown here. The variation in frequency with the frequency droop controller is significantly higher than that with the angle droop controller. The standard deviation for the window shown is 0.153 rad/s with the frequency droop controller, while it is 0.0011 rad/s with the angle droop controller. It can also be seen that the mean frequency deviation is much larger in case of frequency droop than in angle droop. This demonstrates that the angle droop controller generates a substantially smaller frequency variation than the conventional frequency droop controller.

The output power and current of DG-1 is shown in Fig. 30 for both frequency and angle droop controllers. Since the output currents in this figure are essentially the same and the DGs are

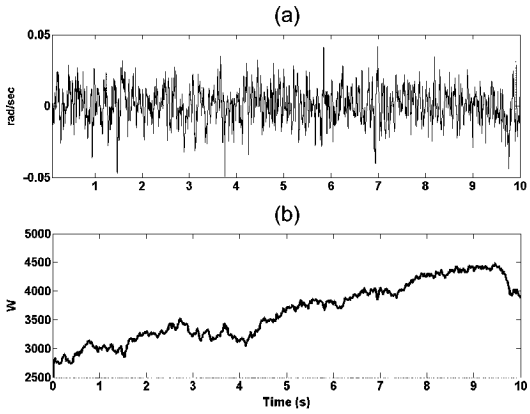

Fig. 29. Frequency deviation with angle droop control. (a) Frequency deviation with angle droop (DG-2). (b) Power output with angle droop (DG-2).

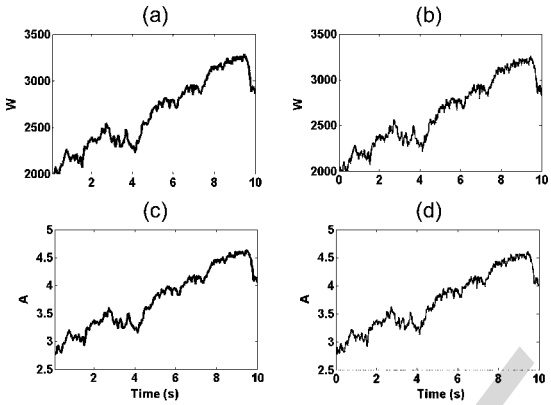

Fig. 30. Output power and current of DG-1 for both droop control methods.

operated at same constant voltage of 1000 V in both cases, the required power of the VSCs is also the same. As the load is not modeled as frequency dependant, the total power being supplied under both control schemes is also closely matched, as evident from Fig. 30. The switching frequency in both the cases is the same. Thus the converter requirements are the same in both the control schemes. For a given frequency error, there will be a finite (proportional) response from the frequency droop controller. In the same situation, the angle droop controller output will continue to ramp until the frequency error is corrected. In normal operation, this will give a superior transient correction term in the angle droop control output, while the steady state power matches the load demand in both control schemes.

APPENDIX B

Some of the simulation results to indicate the accuracy of the proposed control are listed in Table II.

TABLE II
NUMERICAL RESULTS

Case-1		Power	Initial value	Intermediate value	Final value
Section VII.A Load Sharing of the DGs with Utility	Fig. 9	P_1	0.24 MW	0.119 MW	0.24MW
		P_2	0.3 MW	0.15 MW	0.3
		P_T	0.56 MW	0.275 MW	0.56 MW
		P_L	1.1 MW	0.55 MW	1.1 MW
		Q_1	0.45 MVAr	0.23 MVAr	0.45 MVAr
		Q_2	0.55 MVAr	0.272 MVAr	0.55 MVAr
		Q_T	0.98 MVAr	0.5 MVAr	0.98 MVAr
		Q_L	1.98 MVAr	1.0 MVAr	1.98 MVAr
	Fig. 10		Initial value	Intermediate value	Final value
		Capacitor Voltage (kV)	3.501 kV	3.50 kV	3.501 kV
		Angle Controller Output (degree)	-10.8	-8.4	-10.8
Case-2		Power	Initial value		Final value
Section VII.B Change in Power	Fig. 11	P_1	0.131 MW		0.2058 MW
		P_2	0.169 MW		0.2575 MW
		P_T	0.271 MW		0.117 MW
		P_L	0.55 MW		0.55 MW
Supply from Utility		Q_1	0.221 MVAr		0.35 MVAr
		Q_2	0.278 MVAr		0.439 MVAr
		Q_T	0.49 MVAr		0.2 MVAr
		Q_L	0.99 MVAr		0.99 MVAr
Case-3		Power	Initial value		Final value
Section VII.C Power supply from Micro-grid to Utility	Fig. 13	P_1	0.131 MW		0.369 MW
		P_2	0.169 MW		0.461 MW
		P_T	0.281 MW		-0.281 MW
		P_L	0.55 MW		0.55 MW
		Q_1	0.332 MVAr		0.55 MVAr
		Q_2	0.416 MVAr		0.69 MVAr
		Q_T	0.25 MVAr		-0.25 MVAr
		Q_L	0.99 MVAr		0.99 MVAr
Case-Multiple DGs		Power	Initial value	Intermediate value	Final value
Section VIII Real Power Sharing with Four DGs	Fig. 25	P_1	0.0616 MW	0.161 MW	0.0616 MW
		P_2	0.077 MW	0.202 MW	0.077 MW
		P_3	0.0954 MW	0.25 MW	0.0954 MW
		P_4	0.1059	0.277	0.1059
		P_T	0.21 MW	0 21MW	0.21 MW
		P_L	0.55 MW	1.1 MW	0.55 MW

REFERENCES

[1] F. Katiraei and M. R. Iravani, "Power management strategies for a microgrid with multiple distributed generation units," *IEEE Trans. Power Syst.*, vol. 21, no. 4, pp. 1821–1831, Nov. 2006.

[2] M. Reza, D. Sudarmadi, F. A. Viawan, W. L. Kling, and L. Van Der Sluis, "Dynamic stability of power systems with power electronic interfaced DG," in *Proc. Power Systems Conf. Expo. (PSCE'06)*, 2006, pp. 1423–1428.

[3] J. M. Guerrero, L. G. de Vicuna, J. Matas, M. Castilla, and J. Miret, "A wireless controller to enhance dynamic performance of parallel inverters in distributed generation systems," *IEEE Trans. Power Electron.*, vol. 19, no. 5, pp. 1205–1213, Sep. 2004.

[4] M. C. Chandorkar, D. M. Divan, and R. Adapa, "Control of parallel connected inverters in standalone ac supply systems," *IEEE Trans. Ind. Appl.*, vol. 29, no. 1, pp. 136–143, Jan./Feb. 1993.

[5] J. G. Slootweg and W. L. Kling, "Impacts of distributed generation on power system transient stability," in *Proc. IEEE Power Eng. Soc. Summer Meeting*, 2002, vol. 2, pp. 862–867.

[6] L. Yunwei, D. M. Vilathgamuwa, and C. L. Poh, "Design, analysis, and real-time testing of a controller for multibus microgrid system," *IEEE Trans. Power Electron.*, vol. 19, no. 5, pp. 1195–1204, Sep. 2004.

[7] A. L. Dimeas and N. D. Hatziargyriou, "Operation of a multiagent system for microgrid control," *IEEE Trans. Power Syst.*, vol. 20, no. 3, pp. 1447–1455, Aug. 2005.
[8] J. A. P. Lopez, C. L. Moreira, and A. G. Madureira, "Defining control strategies for microgrid islanded operation," *IEEE Trans. Power Syst.*, vol. 21, no. 2, pp. 916–924, May 2006.
[9] S. Chakroborty, M. D. Weiss, and M. G. Simoes, "Distributed intelligent energy management system for a single-phase high-frequency ac microgrid," *IEEE Trans. Ind. Electron.*, vol. 54, no. 1, pp. 97–109, Feb. 2007.
[10] S. M. Brahma and A. A. Girgis, "Development of adaptive protection scheme for distribution systems with high penetration of distributed generation," *IEEE Trans. Power Del.*, vol. 19, no. 1, pp. 56–63, Jan. 2004.
[11] J. C. M. Vieira, W. Freitas, W. Xu, and A. Morelato, "Efficient coordination of ROCOF and frequency relays for distributed generation protection by using the application region," *IEEE Trans. Power Del.*, vol. 21, no. 4, pp. 1878–1884, Oct. 2006.
[12] H. Nikkhajoei and R. H. Lasseter, "Microgrid protection," in *Proc. IEEE Power Eng. Soc. General Meeting*, Tampa, FL, 2007.
[13] H. Al-Nasseri, M. A. Redfern, and R. O'Gorman, "Protecting microgrid systems containing solid-state converter generation," in *Proc. Int. Conf. Future Power Systems*, 2005.
[14] A. Ghosh and A. Joshi, "A new approach to load balancing and power factor correction in power distribution system," *IEEE Trans. Power Del.*, vol. 15, no. 1, pp. 417–422, Jan. 2000.
[15] A. Ghosh, "Performance study of two different compensating devices in a custom power park," *Proc. Inst. Elect. Eng., Gen., Transm., Distrib.*, vol. 152, no. 4, pp. 521–528, Jul. 2005.

Ritwik Majumder (S'07) received the B.E. degree in electrical engineering from Bengal Engineering College (Deemed University), Howrah, India, in 2001 and the M.Sc. (Engg.) degree from Indian Institute of Science, Bangalore, India, in 2004. Since June 2007, he has been pursuing the Ph.D. degree at Queensland University of Technology, Brisbane, Australia.

From July 2004 to November 2004, he was with Tata Motor Engineering Research Centre, Jamshedpur, India. From November, 2004 to January 2006, he was with Siemens Automotive India and from January 2006 to May 2007, he was with ABB Corporate Research Centre, Bangalore, India. His interests are in power systems dynamics, distributed generation, and power electronics applications.

Arindam Ghosh (S'80–M'83–SM'93–F'06) received the Ph.D. degree in electrical engineering from the University of Calgary, Calgary, AB, Canada, in 1983.

He is a Professor of power engineering at Queensland University of Technology (QUT), Brisbane, Australia. Prior to joining the QUT in 2006, he was with the Department of Electrical Engineering at IIT Kanpur, India, for 21 years. His interests are in control of power systems and power electronic devices.

Dr. Ghosh is a fellow of the Indian National Academy of Engineering (INAE).

Gerard Ledwich (M'73–SM'92) received the Ph.D. degree in electrical engineering from the University of Newcastle, Newcastle, Australia, in 1976.

He has been Chair Professor in Power Engineering at Queensland University of Technology, Brisbane, Australia, since 2006. Previously, he was the Chair in Electrical Asset Management from 1998 to 2005 at the same university. He was Head of Electrical Engineering at the University of Newcastle from 1997 to 1998. Previously, he was associated with the University of Queensland from 1976 to 1994. His interests are in the areas of power systems, power electronics, and controls.

Dr. Ledwich is a fellow of I.E.Aust.

Firuz Zare (M'97–SM'06) was born in Iran in 1967. He received the Ph.D. degree in electrical engineering from Queensland University of Technology (QUT), Brisbane, Australia.

He has worked as a Development Engineer and a Consultant in industry for several years. He joined the School of Engineering Systems at QUT in 2006. His research interests are power electronic applications, pulse-width modulation techniques, renewable energy systems, and electromagnetic interferences.